Modified Pyridine-2,6-dicarboxylate Acid Ligands for Sensitization of Near-Infrared Luminescence from Lanthanide Ions (Ln^{3+} = Pr^{3+}, Nd^{3+}, Gd^{3+}, Dy^{3+}, Er^{3+})

Michael R. George†, Paul E Critchley‡, George F. S. Whitehead§, Andrew J. Bailey†, Francesco Cuda†, Benedict N. Murdin‡, Martin C. Grossel†, and Richard J. Curry#

†School of Chemistry, University of Southampton, Highfield, Southampton, SO17 1BJ U.K.

‡Advanced Technology Institute, Faculty of Electronics and Physical Sciences, University of Surrey, Guildford, GU2 7XH U.K.

§Department of Chemistry, University of Manchester, Oxford Road, Manchester, M13 9PL U.K.

#Photon Science Institute and Department of Electrical and Electronic Engineering, University of Manchester, Oxford Road, Manchester, M13 9PL U.K.

Email: mcg1@soton.ac.uk, richard.curry@manchester.ac.uk.

Abstract

A detailed study of the ability of pyridine-2,6-dicarboxylic acid (**1**) and its 4-mono- and 3,4,5-tri-substituted analogues to sensitize emission from Pr^{3+}, Nd^{3+}, Gd^{3+}, Dy^{3+} and Er^{3+} is presented. Sensitization of Ln^{3+} emission was demonstrated via the ligands in all complexes, excluding Gd^{3+}, with emission covering the spectral range from 500 nm to 1850 nm obtained with variation of the Ln^{3+} ion. From the study of the ligand-based photoluminescence obtained from Gd^{3+}-complexes, and the relative ligand and Ln^{3+} emission obtained from the other complexes, the singlet and triplet state energies of complexes of (**1**) are estimated to be at 3.1 eV and 2.6 eV respectively whilst for the 3,5-dibromo-substituted complexes (**4**) they are at 2.9 eV and 2.3 eV. Hypersensitivity of the Er^{3+} $^4I_{15/2} \rightarrow {}^2H_{11/2}$ and $^4I_{15/2} \rightarrow {}^4G_{11/2}$ intra-atomic transitions is also observed in the 4-chloro-substituted (**3**) complex. Enhanced sensitization of Nd^{3+} (ca. 5-fold) and Er^{3+} (ca. 2-fold) near-infrared emission is demonstrated for complexes of (**3**) and (**4**) respectively in comparison with those of (**1**).

Keywords: Lanthanide luminescence, energy transfer, Judd-Ofelt, photoluminescence, organolanthanide.

1. Introduction

Ligand-sensitized emission from the intra-atomic $4f \rightarrow 4f$ transitions of the lanthanide ions (Ln^{3+}) continues to be of significant interest to researchers since its first demonstration ~75 years ago.[1] For those working in a wide range of disciplines this is mainly due to the characteristic spectrally narrow emission obtained from the Ln^{3+} $4f \rightarrow 4f$ intra-atomic transitions and their relatively long radiative lifetime. Following initial demonstration of the process, significant research developing visible emitters (in particular containing Eu^{3+} and Tb^{3+} for red and green emission respectively) for use in displays[2] and as fluorescent markers[3,4] has been undertaken. The complexation of Ln^{3+} with organic ligands also enabled near-infrared (NIR) emission to be obtained from organic systems thus significantly extending their potential application.[5-8] Initial interest in NIR emission was focused on their potential for use in optoelectronic systems in particular utilizing the Er^{3+} $^4I_{13/2} \rightarrow {}^4I_{15/2}$ 1.53 μm emission[9] coinciding with the silica optical fiber low-loss transmission region.[10,11] More recently NIR emitters have become of increasing interest for use as markers in biological systems[12,13] due to the transmission of tissue in the NIR region and also as potential sources for low-cost sensing applications.[14,15]

We have previously outlined the Ln^{3+} excitation mechanism used in these systems in some detail[5] and further reviews are also available.[2,16,17] However, given the scope of this paper we present here a brief summary to aid the presentation and discussion of the results within. Excitation is initiated through the creation of an excited electronic state in the organic ligand most typically via optical absorption. In this case a singlet excitonic state (S_1) is formed which may either relax radiatively (giving ligand-centered fluorescence), undergo intersystem crossing (ISC) to the ligand triplet state (T_1), or recombine non-radiatively via energy transfer to a resonant Ln^{3+} excited $4f$ energy level.[18] ISC is promoted in these systems due to the increased spin-orbit coupling resulting from the presence of the Ln^{3+}, often referred to as the heavy atom effect. As a result, in the absence of any resonant transfer from the S_1 state to the Ln^{3+}, the T_1 state may be efficiently populated. The evolution of the T_1 state then proceeds either via radiative

recombination (giving ligand centered phosphorescence), non-radiative relaxation via energy transfer to the Ln^{3+} ion, or non-radiative relaxation via the excitation of vibrational modes (phonons) of the complex. An excited Ln^{3+} state, created via energy transfer from the ligand or via direct absorption of a photon, will relax via radiative or non-radiative intra-atomic relaxation. This behavior is dependent upon the vibrational properties of the Ln^{3+} host, relative 4*f* intra-atomic energy level separation and spin selection rules for the parity forbidden $4f \rightarrow 4f$ transitions. It is due to the forbidden nature of the $4f \rightarrow 4f$ transitions that sensitization via the organic ligand is in general significantly more efficient than direct optical excitation of the Ln^{3+}.

In order to obtain efficient emission from the sensitized Ln^{3+}, its local environment must be carefully designed, taking into account both the local phonon energy of the complex and the 8-9 coordination requirement of the ion. If the latter is not fully satisfied, it is common for solvent molecules (water, methanol etc.) to be incorporated into the complex to achieve this. In general such inclusion results in significant quenching of the Ln^{3+} emission, in particular at longer wavelengths in the NIR, via non-radiative coupling to the solvent vibrational modes. This is exemplified in the archetypical complex erbium *tris*(8-hydroxyquinoline), often cited as the benchmark complex in recent studies of Er^{3+} organolanthanide 1.53 μm emission, which is only 6-coordinated.[9] Strategies to overcome this often involve the coordination of 'neutral ligands' such as the use of phenanthroline and bathocuproine.[2] However, these ligands can reduce the efficiency of sensitization via competitive absorption of incident photons, providing a route for back-transfer of energy from the Ln^{3+}, and by increasing the local phonon energy.[19] Additionally, they reduce the symmetry of the complex which can impact on the fine structure of the $4f \rightarrow 4f$ emission and effect the crystallization of the complexes.

A class of complexes that remove the requirement for neutral ligands are those based on the use of pyridine 2,6-dicarboxylate (dpa-**1**) and its 4-mono- and 3,4,5-trisubstituted analogues (**2 - 4**) which are able to fully satisfy the coordination requirements of the Ln^{3+} (Figure 1). The complexes of Tb(**1**)$_3$ and its analogues were originally studied by Lamture et al.[20] and followed up in our previous report of Eu(**1**)$_3$ and its

similar analogues.[21] Their respective green and red emission, long radiative lifetime (μs), and solubility in water make these complexes of interest for use as luminescent probes in aqueous environments[22,23]. Given the promise demonstrated by these visible emitting complexes it is of interest to study NIR emitters as further applications exist in this spectral region, for example in telecommunications, sensing and biological systems that are themselves transparent in this region. Furthermore, (**1**) only occurs naturally in bacterial spores such as Bacillus anthracis and hence is of significant interest for the detection of biological agents and for the study of life in extreme environments.[24-27] The attraction of these complexes is also enhanced by the ability to attach additional functional groups to the 4-position of the pyridine ring.[28,29] However, such studies have typically been restricted to either Eu^{3+} or Tb^{3+} and involved modification of the 4-position[30-35]. For the development of efficient NIR emitting complexes the 3- and 5-positions must also be modified in order to reduce the local phonon energy which leads to deactivation of the Ln^{3+}. It is therefore essential that the full family of reference complexes are studied to provide a basis for future work in this area.

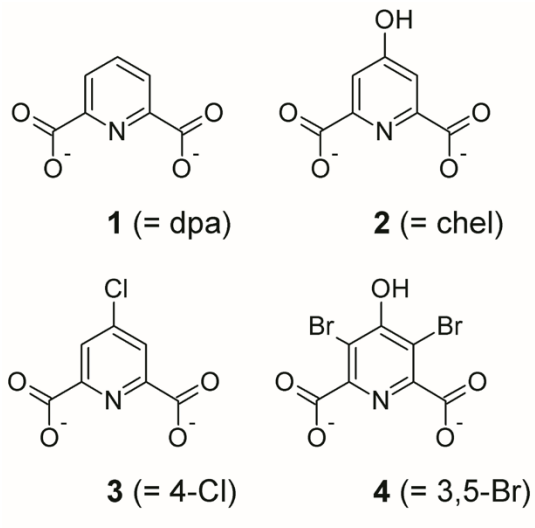

Figure 1. Structure of ligands used to form complexes of Pr, Nd, Gd, Dy and Er.

In this paper we report a detailed study of Pr^{3+}, Nd^{3+}, Gd^{3+}, Dy^{3+}, and Er^{3+} complexes of (**1** - **4**) thus providing a comprehensive foundation for the further development of this family of organolanthanide molecules in conjunction with previous studies on Tb^{3+} and Eu^{3+}.[20,21] The preparation and

characterization of each complex is provided including detailed optical spectroscopic characterization of both visible and NIR absorption, photoluminescence (PL) and PL excitation (PLE) spectra. The PL lifetime and PL quantum efficiency (PLQE) are provided, where possible, along with the results of Judd-Ofelt modelling.[36-38] The characterization of Gd^{3+} complexes is presented first as the absence of intra-atomic transitions in the spectral region of interest allows the effect of the Ln^{3+} on the ligand optical properties to be studied. Following this we present the remaining complexes in order of increasing atomic weight of the Ln^{3+}.

2. Experimental Section

^{1}H and ^{13}C NMR spectra were recorded on a Bruker Advance 300 or a Bruker DPX 400 spectrometer. Chemical shifts (δ) are quoted relative to residual solvent peaks. ^{13}C NMR spectra were fully proton decoupled. Peaks are quoted in chemical shift, ppm (δ): (s) singlet, (d) doublet, (t) triplet, (q) quartet, (m) multiplet. Coupling constants (J) are quoted in hertz. Infrared spectra were obtained using a Golden Gate sampling attachment on a Mattson Satellite 3000 Fourier transform infrared instrument. Masses are quoted as the lowest isotopic mass (for instance, ^{35}Cl and ^{79}Br if these elements are involved). For compounds that were soluble in methanol, electrospray (ES) mass spectra were recorded on a Micromass Platform II single-quadrupole mass spectrometer. The instrument is calibrated with a mixture of sodium and cesium iodide. The operating conditions were as follows: capillary, 3.50 kV; HV lens, 0.5 kV; cone voltage, 20 V; source temperature, 110 °C; ES eluant, 100 % acetonitrile at 100 $\mu Lmin^{-1}$; nitrogen drying gas, 300 Lh^{-1}; and nebulizing gas, 20 Lh^{-1}. Ten-microliter injections of ~1-10 μLmL^{-1} solutions were made using a Hewlett-Packard HP1050 autosampler. Negative-ion data were recorded under identical conditions except for different polarity voltages and capillary voltages of -3.0 kV. Elemental analyses were performed by Medac Ltd. of Alpha 319, Chobham Business Centre, Chertsy Road, Chobham, Surrey, GU24 8JB, U.K. Melting points were measured on an Electrothermal melting point apparatus and are uncorrected. Single crystal X-ray diffraction (ScXRD) data were collected using a Rigaku Fr-X rotating anode diffractometer equipped with VariMax-DW^{TM} optics, an XtaLAB AFC11 quarter-χ

goniometer, using CuKα radiation (1.54184 Å) at either 100 or 150K (see supplementary information for refinement details). All of the solvents and reagents used were of reagent grade, obtained from Aldrich, and were used without any further purification except where specified.

2.1 Preparation of Ligands. Chelidamic acid ($2 \cdot 2H^+$), 4-chloropyridine-2,6-dicarboxylic acid ($3 \cdot 2H^+ + 2H_2O$), and 3,5-dibromo-4-hydroxypyridine-2,6-dicarboxylic acid dihydrate ($4 \cdot 2H^+ + 2H_2O$) were all prepared and characterized as we have previously reported.[21]

2.2 Preparation of Complexes. In a typical preparation, a solution of (**1**) (3.0 mmol) in methanol (50 ml) was added to a stirred solution of rare earth acetate (1.0 mmol) in methanol (50 ml). The solutions became turbid when mixed, but upon addition of triethylamine (6.0 mmol) the suspension dissolved and formed a clear, colorless solution. The reaction was stirred at room temperature for 2 days and then the solvent was evaporated under reduced pressure and the residue (usually a sticky film) was triturated in acetone (10ml) to yield a powder which was crystallized from hot methanol unless otherwise stated. Full details of the synthesis and chemical characterization of each complex are provided in the supplementary information.

2.3 Spectroscopic Measurements. UV-Vis-NIR absorption spectra of each complex were obtained using low and high concentration solutions (typically ~0.1 mM and 10 mM) in methanol (unless stated otherwise) using UV-quartz 10-mm cuvettes. The high concentration samples were used to measure the Ln^{3+} intra-atomic $4f \rightarrow 4f$ transitions. Absorption spectra were obtained using a Varian Cary 500 spectrophotometer with a spectral resolution of 0.1 nm over the wavelength range of 190-2000 nm. PL was excited from powder samples held between quartz slides using 351 or 458 nm Ar^+ laser excitation (Coherent Innova I308C). The excitation was modulated using an optical chopper to enable lock-in amplification (Signal Recovery DSP 7265). PL spectra were recorded with a conventional set-up consisting of a monochromator (1200 lines mm^{-1} blazed at 500 nm and 600 lines mm^{-1} blazed at 1μm; Bentham TMc300-C) and detected using a Si or InGaAs photodiode (Newport 818-SL or 818-IG). Long-pass filters were used as appropriate to remove scattered laser light. All spectra have been corrected for

the optical response of the system and any filters used. PLE spectra were obtained using the output of a Nd:YAG pumped tuneable optical parametric oscillator (Newport VersaScan OPO) and UV frequency doubler (Newport UV-Scan). Signal and idler outputs were selected and rejected as appropriate. To remove the effect of pulse-to-pulse energy variation signal averaging was used along with a wavelength calibrated beam sampler system to obtain the incident energy at each wavelength. The same system was used to obtain the PL lifetime (τ_{meas}) data along with visible (S-20) and liquid nitrogen cooled NIR photomultiplier tubes (PMTs) coupled to a fast oscilloscope. PLQE studies were undertaken using the method described by de Mello by modifying the PL set-up to incorporate an integrating sphere.[39]

2.4 Judd-Ofelt Modelling The experimental line strength, S_{EDmeas}, of each $J \rightarrow J'$ transition was determined using eq 1:

$$S_{EDmeas}(J:J') = \frac{3ch(2J+1)}{8\pi^3 e^2 \bar{\lambda}} n \left(\frac{3n}{n^2+2}\right)^2 \int_{manifold} \sigma(\lambda) d\lambda \qquad (1)$$

The constants and parameters within eq 1 are defined as: c is the speed of light in vacuum, h is Plank's constant, J is the total angular momentum of the initial 4f state, e the electronic charge, $\bar{\lambda}$ is the average wavelength of the transition, n the refractive index, and $\sigma(\lambda)$ the absorption cross-section. The Judd-Ofelt parameters, Ω_λ, were then obtained by substitution of the calculated line strengths, S_{EDcalc}, (eq 2), with S_{EDmeas}, and least-squares fitting as described elsewhere.[21] The values of the doubly reduced matrix elements of the intermediate coupling scheme, $\left|\langle f^n[SL]J|\mathbf{U}^{(\lambda)}|f^n[S'L']J'\rangle\right|^2$, in eq 2 were taken from those previously tabulated.[40-43] Further details of the Judd-Ofelt modelling and validation are provided in the supplementary information (and supplementary information Tables S3-5).

$$S_{EDcalc}(J:J') = \sum_{\lambda=2,4,6} \Omega_\lambda \left|\langle f^n[SL]J|\mathbf{U}^{(\lambda)}|f^n[S'L']J'\rangle\right|^2 \qquad (2)$$

The Einstein coefficient $A(J' \rightarrow J)$ for transitions of interest were then obtained using eq 3 assuming a negligible magnetic dipole contribution is each case.

$$A(J' \rightarrow J) = \frac{64\pi^4 e^2}{3h(2J'+1)\bar{\lambda}^3}\left[n\left(\frac{n^2+2}{3n}\right)S_{EDRad}(J':J) + n^2 S_{MDRad}(J':J)\right] \qquad (3)$$

Using eq 3 the radiative lifetimes $\tau_{calc} = \left[\sum_J A(J':J)\right]^{-1}$ and branching ratios $\beta_{J'\rightarrow J} = \frac{A(J':J)}{\sum_J A(J':J)}$ were determined with the PLQE estimated using $\eta = \tau_{meas}/\tau_{calc}$.

3. Results

3.1 Gd^{3+}-Complexes

The absorption spectra of Gd(**1-4**)$_x$ are presented in Figure 2(a). As previously reported for Tb- and Eu-analogues[15,16] a bathochromic shift of the absorption edge is seen with substitution of the pyridine 4-position in the order H > Cl > OH with the magnitude of the shift being similar to that seen for Tb. Upon Br-substitution at the 3- and 5-positions of the pyridine ring, the shift due to OH substitution at the 4-position is dramatically enhanced as was seen for Eu(**1-4**)$_x$.[21] This is accompanied by a reduction in absorption at ca. 325 nm compared to the other complexes at ca. 280 nm. The substitution of the 4-position does not significantly alter the ligand absorption strength at ca. 280 nm in Gd(**1-3**)$_3$ (inset Figure 2(a)).

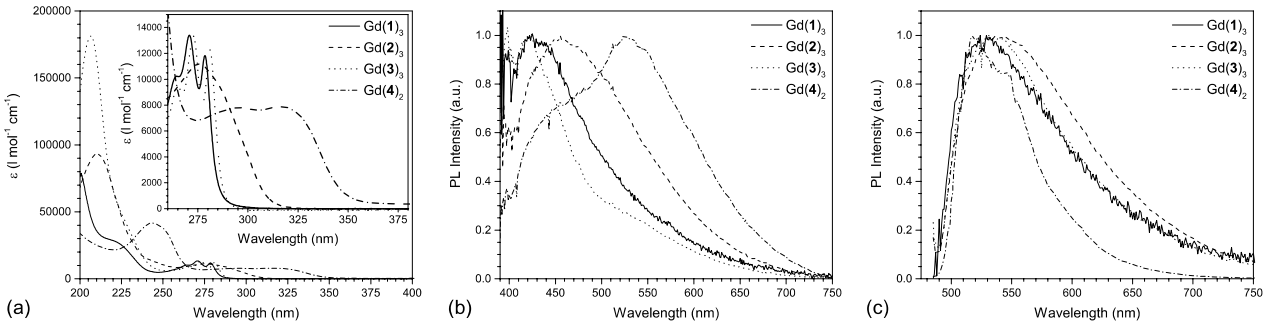

Figure 2. Absorption spectra in methanol (a) and 351 nm excited (b) and 458 nm excited (c) powder photoluminescence spectra (bottom) of gadolinium(III) *tris*(pyridine-2,6-dicaroxylic acid) and its analogues [Gd(**1-4**)$_x$].

The absorption of Gd(**1**)$_3$ closely matches that of the dipicolinate anion (DPA^{2-}) with a very weak absorption in the 300 – 320 nm region followed by its maximum at ca. 280 nm coinciding with the predictions of density functional theory (DFT) modeling of DPA^{2-}.[44] Chlorination of the ligand leads to a net reduction in the charge density in the pyridine ring resulting in the small observed blue-shift of the absorption spectrum. In contrast, substitution with OH increases the ring charge density and is thus responsible for the observed red-shift in absorption. The enhancement of the red-shift with further bromination may be due to an increase in the oscillator strength of direct singlet-triplet state absorption. The lowest triplet state energies calculated using DFT of DPA were reported[44] to be at 318, 352, and 355 nm below the lowest (dipole allowed) singlet energy at ca. 298 nm supporting experimental observations.[45] Allowance for a similar energy difference between the singlet and triplet states of DPA^{2-} (a ca. 50 nm red-shift) would explain the significant extension of the absorption in the case of Gd(**4**)$_2$.

Studies of Lu^{3+}-based 'push-pull' donor-π-conjugated DPA ligands (Lu^{3+} used in place of Gd^{3+} to allow improved ^{1}H and ^{13}C NMR characterization) showed that complexation only resulted in a small blue-shift of the ligand absorption and emission.[28] Additionally, exchange of Lu^{3+} for other Ln^{3+} ions (Eu, Nd and Yb) has only a further minor affect these properties. However, in these reported systems the optical properties are significantly dependent on the formation of charge-transfer states between the DPA and donor π-systems.

Inspection of the higher energy absorption reveals significant variation in the intensity of the absorption with Gd(**1-3**)$_3$ each displaying a shoulder at ca. 230 nm with a second peak at ca. 210 nm. In contrast Gd(**4**)$_2$ displays an almost uniform absorption for up to 50 nm from its first peak at ca. 325 nm. At energies above this a second major peak is found at ca. 250 nm, in contrast to the other complexes which exhibit a localized minimum in this region, before increasing in intensity again.

Figure 2(b) shows the PL spectra of Gd(**1**-**4**)$_x$ excited at 351 nm and normalized to the maximum of the broad emission observed from each complex. At wavelengths below ca. 390 nm the spectra exhibit a large noise level due to the correction applied to compensate for the use of a ca. 400 nm long-pass filter to

prevent scattered excitation light entering the detection system. This may also affect the observed PL maximum which has (for DPA) previously been reported at ca. 400 nm.[46] We note from the absorption spectra that Gd(**1-3**)$_3$ exhibits an exceptionally weak absorption at the 351 nm excitation wavelength yet at the excitation power used (ca. 1.5 mW mm^{-2}) each sample could be clearly seen to luminesce by eye. Inspection of the PL spectra shows each ligand displaying broad emission peaking at ca. 420 nm for Gd(**1**)$_3$ and Gd(**3**)$_3$ shifting to ca. 455 nm upon substitution of the pyridine 4-position with OH. The similar peak positions for Gd(**1**)$_3$ and Gd(**3**)$_3$ might be expected given the similarity of their absorption spectra. However, their PL behavior deviates significantly on the low-energy side of the emission peak with Gd(**1**)$_3$ exhibiting an enhanced low energy tail and shoulder centered at ca. 440 nm. Substitution with OH to form Gd(**2**)$_3$ causes a further extension of the low energy tail, which now extends across the entire visible spectrum, along with the above noted redshift in the emission peak which is in line with the observed bathochromic shift observed in the absorption spectrum. Upon the addition of Br to form Gd(**4**)$_2$ the low energy tail is again extended with the main emission peak occurring at ca. 530 nm with the presence of a higher energy peak centered at ca. 450 nm clearly evident. A good fit of this spectrum using two Gaussian peaks is obtained with the peaks found to be at 531 nm (2.33 eV) and 430 nm (2.89 eV) (supplementary information Figure S2(a)). Likewise successful fitting of the Gd(**1-3**)$_3$ PL spectra could be obtained using a sum of two Gaussians. In doing so it is noted that the high energy tail of these spectra is affected by the long-pass filter cut-off leaving only a relatively small usable data set for fitting on this high energy side of the PL peak. As a result the significance of the resulting fits for Gd(**1-3**)$_3$ cannot be fully quantified. Qualitatively however the fitted Gaussian peak positions were found to vary with ligand substitution in the same manner observed for the shift in absorption peak maximum.

The 351 nm excited luminescence obtained from these complexes can be used as a good approximation of the position of the electronic manifolds for the complexes of the other Ln^{3+} ions reported in this study. In each complex spin-orbit (**L.S**) coupling, enhanced by the presence of Gd^{3+}, is likely to occur, increasing intersystem crossing (ISC) between the ligand singlet and triplet states. Supporting this is the large Stokes

shift, ca. 1.5 eV, observed for Gd(**1-3**)$_3$ which is reduced to ca. 0.75 eV for Gd(**4**)$_2$ due to the significant redshift of its absorption. As a result, these spectra indicate the lowest energy states from which sensitization of Ln^{3+} may take place although they do not rule out energy transfer from higher energy ligand states that may compete with the ISC rate as observed in similar systems. Using the fitted Gaussian peaks obtained from the PL spectrum of Gd(**4**)$_2$ we give a tentative assignment of the ca. 430 nm (2.89 eV) emission to the singlet state and the ca. 531 nm (2.33 eV) emission to the triplet state of Gd(**4**)$_2$. Based on the absorption and PL spectra in Figure 2(a) and (b) the energy of these states is likely to be higher for Gd(**1-3**)$_3$ (which we discuss later) thus they represent the lowest energy for the series of complexes studied. Furthermore, the enhanced **L.S** coupling expected in Gd(**4**)$_2$ due to the presence of the two Br atoms would increase the ISC and enhance the triplet emission in agreement with the observed PL spectrum.

To provide further information regarding this assignment Figure 2(c) shows the 458 nm excited PL spectra obtained from Gd(**1-4**)$_x$. This excitation energy lies well below the singlet level and has a very small absorption coefficient as can be seen in the absorption spectra (Figure 2(a)). As a result the emission obtained, assuming our assignment to be valid, must be from direct excitation of the triplet state as discussed above. It can be seen that the PL spectra of Gd(**1-3**)$_3$ are all very similar, however, curiously that of Gd(**4**)$_2$ is significantly narrower than might be expected. The use of the long-pass filter prevents accurate determination of the PL peak position for comparison with the predicted triplet state energies obtained by fitting the 351 nm excited PL spectrum. However, a comparison of these spectra with the low energy Gaussian obtained from fitting 351 nm excited Gd(**4**)$_2$ PL spectrum is provided in supplementary information Figure S2(b). These can be seen to be in reasonable agreement in terms of the peak position and low-energy spectral range. The anomalous behavior of the 458 nm excited Gd(**4**)$_2$ PL low-energy tail (in comparison to the 351 nm excited spectrum) is reproducible and may be related to the incomplete coordination of the complex.

PLE spectra of each complex were obtained, measured at 550 nm, and are shown in supplementary information Figure S3. The PLE spectra of Gd(**1**,**3**)$_x$ are found to be similar with evidence of broad peaks centered at ~250, 325 and 425 nm identifiable. Interestingly, in the PLE spectrum of Gd(**2**)$_3$ these features are not easily identifiable with the strong absorption observed at ~210 nm not being translated into the PLE spectrum. In the case of Gd(**4**)$_2$ the PLE spectrum shows a strong edge at ~400 nm whose fitting would suggest gives a peak at ~500 nm. The presence of this peak supports the proposition that when exciting at wavelengths above ~400 nm direct excitation of the triplet state is occurring.

To assist in the interpretation and discussion of the optical properties of the lanthanide complexes presented within, Figure 3 shows a schematic of the intra-atomic 4*f* energy levels of the Ln^{3+} ions reported in this study (and within our previous study of Eu^{3+}) along with the singlet and triplet states energy proposed above and the laser excitation energies used. For the case of Gd(**1**-**4**)$_x$ it is clear that no energy transfer to any Gd^{3+} intra-atomic 4*f* level may occur, hence confirming that the above reported emission must be ligand based. Measurement of the PL decay of Gd(**1**-**4**)$_x$ under 420 nm excitation (2.95 eV) at emission wavelengths over the range of 480 nm to 750 nm are shown in supplementary information Figure S4. The PL lifetimes obtained are tabulated in supplementary information Table S6 and reveal a small reduction from ~10 ns for Gd(**1**)$_3$ to ~8 ns upon substitution. Such lifetimes are further evidence for strong **L.S** coupling allowing the fast radiative recombination of the excited triplet state. It can also be seen that although the excitation wavelengths chosen (based on the limited range afforded by an Ar^+ laser) for the PL studies do not coincide with the major absorption bands of the ligands, they are suitably placed above and below the singlet states to provide considerable insight into the excitation and energy transfer mechanisms in play within these complexes.

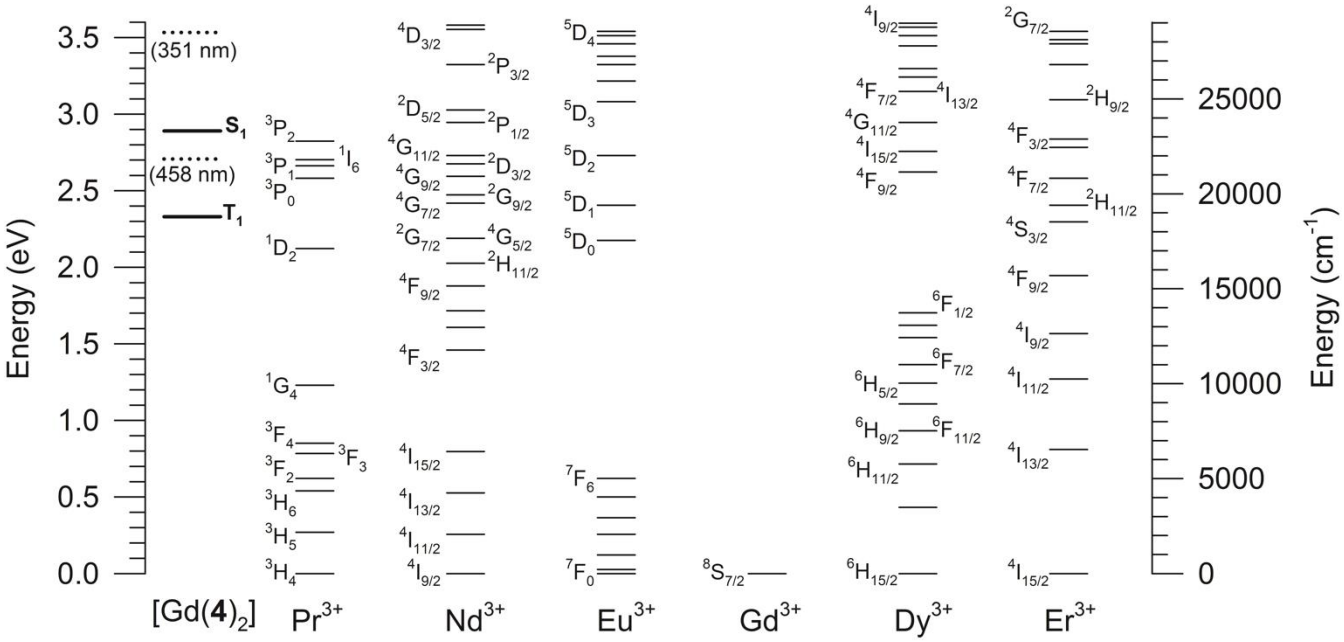

Figure 3. Intra-atomic 4*f* energy levels of various Ln^{3+} ions[40-43] and the relative positions of the singlet and triplet ligand states of Gd(**4**)$_2$ and the laser excitation energies used.

3.2 Pr^{3+}-Complexes

Figure 4(a) shows the absorption and PL spectra of Pr(**1**-**4**)$_3$ noting that Pr(**3**)$_3$ was found to be insoluble in a wide range of solvents hence its absorption spectrum is not available. In comparison with the Gd(**1**-**4**)$_x$ analogues, the only significant change in the ligand absorption is in that of Pr(**4**)$_3$ which whilst still extending to ca. 360 nm has its maximum at ca. 290 nm, shifted from 325 nm as observed in Gd(**4**)$_2$. In addition to the shift, shoulders are clearly visible in the low energy tail at ca. 315 and 340 nm. Previous reports have assigned absorption above 400 nm in Pr^{3+}-complexes and salts to a ligand-to-metal charge transfer (CT) process in particular at ca. 250 nm.[47,48] In the LuI_3:Pr^{3+} system an $I^- \rightarrow Pr^{3+}$ CT band at ca. 320 nm has also been proposed whilst in $LaBr_3$:Pr^{3+} systems a $Br^- \rightarrow Pr^{3+}$ CT band occurs at ca. 250 nm.[48] However, based on these reports the additional features observed in the absorption spectrum of Pr(**4**)$_3$ appear to be at too long a wavelength to be definitively assigned to such a phenomenon.

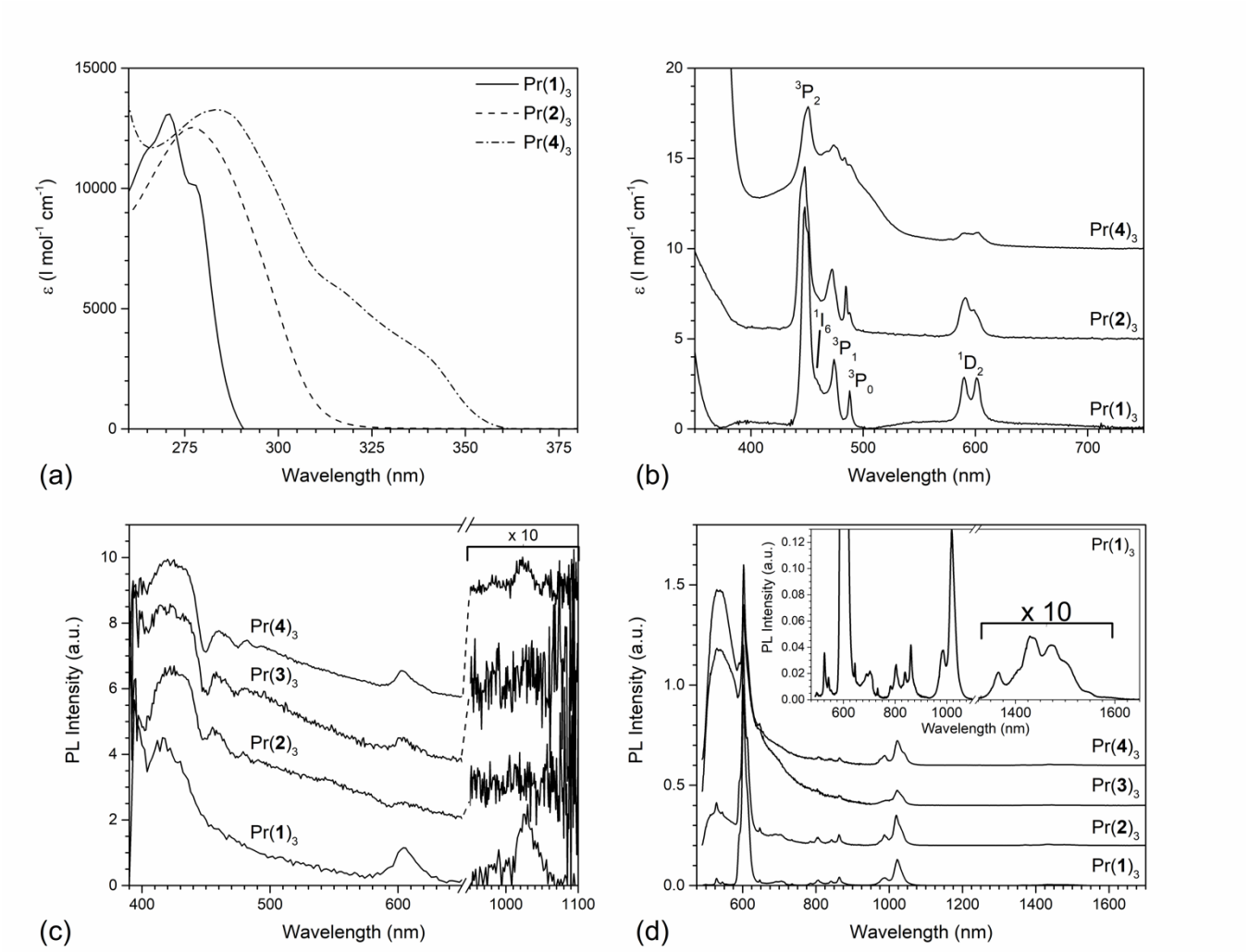

Figure 4. Absorption spectra in DMSO (except Pr(**2**)$_3$ in H_2O) (a) and (b), and 351 nm and 458 nm excited powder photoluminescence spectra ((c) and (d) respectively) of praseodymium(III) *tris*(pyridine-2,6-dicarboxylic acid) and its analogues [Pr(**1**-**4**)$_3$]. The Pr^{3+} 4*f* intra-atomic absorption transitions identified occur from the $^3H_4$ ground state to those indicated. Further transitions are identified in Figure 5(b) and supplementary information Figure S5.

To obtain the absorption spectra due to Pr^{3+} 4*f* transitions as shown in Figure 4(b) concentrated solutions were studied. The spectra of Pr(**2**)$_3$ and Pr(**4**)$_3$ have been vertically offset for clarity by 6 and 12 *l*mol^{-1}cm^{-1} respectively. The first Pr^{3+} absorption peak common to all the complexes is observed at ca. 600 nm and is assigned to the $^3H_4 \rightarrow {}^1D_2$ transition. This can be clearly seen to consist of a doublet (at the resolution used for these measurements) which reduces in intensity as ligand substitution proceeds and appears to

be broadened in the case of Pr(**4**)$_3$. This peak is followed by a series of further absorption transitions in the 435 – 500 nm region which are attributed to the Pr^{3+} $^3H_4 \rightarrow {}^3P_0$, $^3P_1$, $^1I_6$, and $^3P_2$ transitions. At wavelengths above 400 nm the emergence of ligand-based absorption begins to dominate.

In the NIR a very weak absorption at ca. 1015 nm was observed in Pr(**1**)$_3$ due to $^3H_4 \rightarrow {}^1G_4$ transitions, shown in supplementary information Figure S5. This was not detectable in Pr(**4**)$_3$ and although a peak in Pr(**2**)$_3$ was detected it is not significantly larger than the noise level of the spectrum. At longer wavelengths a stronger absorption due to $^3H_4 \rightarrow {}^3F_4$ and $^3H_4 \rightarrow {}^3F_3$ transitions is found at ca. 1450 nm. This absorption was not detectable in Pr(**2**)$_3$ or Pr(**4**)$_3$ presumably due to the presence of the OH group introduced into the ligand interfering with the spectrum.

The 351 nm excited PL spectra are shown for all four complexes Pr(**1**-**4**)$_3$ in Figure 4(c) normalized to the intensity at 600 nm and offset for clarity. From the absorption spectra (and Pr^{3+} energy level structure; Figure 3) it is clear that this excitation wavelength can only excite the complex ligands and not the Pr^{3+} directly. Each complex exhibits broad PL peaking at ca. 420 nm which is similar to that observed for Gd(**1**-**4**)$_x$. This similarity of the PL observed from each complex, in particular in the low energy tail at ca. 500 nm, is however in contrast to the differences observed between Gd(**1**-**4**)$_x$. The CT discussed above has been reported to lead to a broad emission centered at ca. 400 nm. This at first appears to be remarkably similar to the PL observed under 351 nm excitation and might lead to the ascribing of the origin of this emission as due to the $^1S_0 \rightarrow {}^1I_6$ CT state.[48] However, the similarity to the emission observed from Gd(**1**-**4**)$_x$, and the other complexes discussed below, does not support this assignment hence the origin is, we believe, ligand based.

Inspection of the PL within the spectral region between 430 nm and 500 nm of Pr(**2**-**4**)$_3$ reveals clear features due to absorption of the PL by the Pr^{3+} exciting the $^3P_{0,1,2}$ and $^1I_6$ levels (and incidentally offers an effective absorption spectrum for Pr(**3**)$_3$). This is evidenced by the characteristic ‘notches’ in what would otherwise be a smooth PL spectrum (c.f. Figure 4c and Figure 2b). This can only occur following the radiative recombination of a ligand exciton, which itself therefore precludes that particular exciton

having undergone direct energy transfer to the Ln^{3+} ion. This then results in emission from the Pr^{3+} being observed at ca. 600 nm which we assign to $^1D_2 \rightarrow {}^3H_4$ and $^3P_0 \rightarrow {}^3H_6$ transitions and at ca. 1020 nm assigned to the $^1G_4 \rightarrow {}^3H_4$ transition, and some weak emission at ca. 985 nm due to the $^1D_2 \rightarrow {}^3F_4$ transition. Similar absorption features are not as obvious in the PL spectrum of Pr(**1**)$_3$ yet Pr^{3+} emission is observed with increased intensity. This may imply that a ligand-to-Pr^{3+} energy transfer process is responsible for Pr^{3+} excitation in Pr(**1**)$_3$ rather than simple reabsorption of ligand PL.[49] We will discuss the implications of this in more detail below. We also observe an increase of ca. 5% in the relative strength of the emission at ca. 600 nm in comparison with that at ca. 1020 nm when comparing Pr(**1**)$_3$ and Pr(**4**)$_3$ (supplementary information Table S7). Emission at ca. 600 nm precludes subsequent emission at ca. 1020 nm (Figure 5(a)), hence this implies that the probability of radiative emission from the $^3P_0 \rightarrow {}^3H_6$ and/or the $^1D_2 \rightarrow {}^3H_4$ transitions has increased in these complexes despite the fact that the ligands do not fully coordinate the Pr^{3+} ion.

Considering now the 458 nm excited PL spectra presented in Figure 4(d) it is immediately apparent that the Pr^{3+} emission is significantly enhanced. Again, we have normalized the spectra at 600 nm and offset them for clarity. The 458 nm excitation can be directly absorbed by the Pr^{3+} $^1I_6$ energy level and, as observed for Gd(**1**-**4**)$_x$, may also excite the ligand triplet state leading to the broad ligand emission observed from Pr(**2**-**4**)$_3$. It can be seen that the intensity of the ligand emission in comparison with the Pr^{3+} 600 nm emission significantly increases with substitution of the ligand. This cannot be associated with the increased absorption of the ligand at 458 nm because Pr(**3**)$_3$ exhibits strong ligand emission despite the ligand exhibiting a lower absorption compared to (**2**) for example (Figure 2(a)). We therefore may infer that strong energy transfer from ligand to Pr^{3+} is occurring in Pr(**1**)$_3$ which decreases upon substitution. Such behavior may be reconciled with the triplet energy level being higher in the case of Pr(**1**)$_3$ favoring coupling to the Pr^{3+} $^3P_0$ energy level via a Förster process ($|\Delta J| = 4$).[50] As the triplet energy reduces with substitution this coupling is reduced leading to the observed increase in ligand PL.

The relative intensities of the Pr^{3+} emission for Pr(**1-4**)$_3$ are provided in supplementary information Table S8.

We can invoke a similar argument to explain the apparent enhancement of the Pr^{3+} emission upon 351 nm excitation in Pr(**1**)$_3$ and Pr(**4**)$_3$ compared to Pr(**2-3**)$_3$ (Figure 4(c)). In Pr(**1**)$_3$ the singlet state will lie above the $^3P_2$ energy level whilst the singlet state of Pr(**4**)$_3$ is in close resonance. This will result in increased ligand to Pr^{3+} energy transfer in the latter ($|\Delta J| = 2$) giving the observed Pr^{3+} PL, whilst as discussed above, Pr(**1**)$_3$ is able to sensitize the Pr^{3+} via its triplet state. For the remaining complexes their singlet states lie too high to enable sensitization via the $^3P_2$ state, whilst their triplet states lie too low to allow sensitization via the $^3P_0$ level. This explains the significantly reduced Pr^{3+} emission in Pr(**2-3**)$_3$ compared to Pr(**1**,**4**)$_3$ under 351 nm excitation.

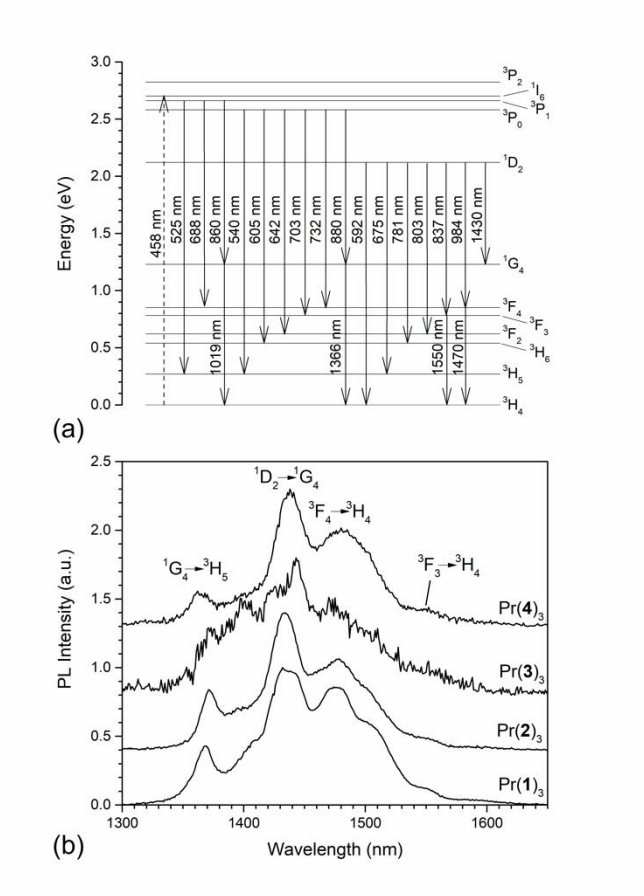

Figure 5. Schematic energy level diagram for Pr^{3+} showing the radiative transitions observed from Pr(**1**)$_3$ under 458 nm excitation (a). The 458 nm excited near infrared PL of Pr(**1-4**)$_3$ (b).

The inset into the 458 nm excited PL spectra (Figure 4(d)) shows a detailed PL spectrum for Pr(**1**)$_3$. The spectral resolution combined with the relatively strong PL intensity allows us to clarify the assignment of intra-atomic transitions for each of the observed peaks which previously have been uncertain for some emission peaks. We show schematically in Figure 5(a) the energy level structure of the Pr^{3+} and are able to assign each of the observed PL peaks and shoulders observed from Pr(**1**)$_3$ under 458 nm excitation (Figure 4(d)). The highest energy emission at ca. 528 nm is due to the $^3P_1 \rightarrow {}^3H_5$ transition and is also observed for Pr(**2**)$_3$ coinciding with the ligand PL maximum. It is possible that this transition is also present in Pr(**3**-**4**)$_3$, although the additional ligand emission makes confirmation difficult. The observation of PL originating from the $^3P_1$ level is perhaps unexpected as fast non-radiative relaxation to the $^3P_0$ level would normally be expected. However, emission is also observed at 688 nm and 860 nm which could only originate from the $^3P_1$ level due to the proximity of neighboring emission assigned to emission from the $^3P_0$ level (e.g. 700 nm and 880 nm emission). It is noticeable that no such emission is observed upon excitation 351 nm hence it is likely that we only observe the emission from the $^3P_1$ level under the direct Pr^{3+} pumping provided by the 458 nm laser excitation. Emission from the $^3P_0$ level is observed due to transitions to all lower energy levels except for the $^3P_0 \rightarrow {}^3H_4$ which at ca. 480 nm lies below the cut-off of the optical filters used and the $^1D_2$ level. A small peak is visible at ca. 495 nm which could be related to such a transition although this cannot be unambiguously confirmed. The emission observed from the $^3P_1$ and $^3P_0$ levels at 860 nm and 880 nm is of particular significance as it populates the $^1G_4$ energy level which will be discussed below.

Emission is also observed originating from the $^1D_2$ level, most probably populated via non-radiative relaxation of the higher levels due to the small energy gap separating them. Emission is observed due to transitions to all lower lying energy levels, again including to the $^1G_4$, which we believe has not been previously reported in organolanthanide complexes. This results in an emission peak centered at 1430 nm with the longer wavelength peaks at 1470 nm and further shoulders observable out to 1550 nm assigned

below. The result of this is that we now have three confirmed radiative pathways leading to population of the $^1G_4$ level.

The populated $^1G_4$ level undergoes radiative relaxation to the $^3H_4$ level emitting at ca. 1019 nm as previously reported. We also observe emission at 1366 nm due to $^1G_4 \rightarrow {}^3H_5$ level, a commonly used lasing transition in optical amplifiers, again not reported for such complexes previously. To complete the assignment of the broad near infrared emission we assign the PL peak at 1470 nm to the $^3F_4 \rightarrow {}^3H_4$ transition and the 1550 nm PL observed as a shoulder to the $^3F_3 \rightarrow {}^3H_4$. The combination of the above described long wavelength emission results in broad near infrared emission spanning the technologically significant wavelength range of 1330 nm to 1600 nm.

Whilst we have focused on the NIR emission obtained from Pr(**1**)$_3$ in the above discussion we also observe similar PL from Pr(**2**-**4**)$_3$ as shown in Figure 5(b). Each spectrum has been normalized to its peak intensity ca. 1430 nm and offset for clarity. The effect of placing the OH group at the 4-position of the pyridine ring is to slightly reduce the emission intensity as indicated by the increase in each spectrum's noise level. It is observed that, although the relative visible emission at ca. 600 nm originating from the Pr^{3+} reduces with ligand substitution of (**1**) with (**4**), the NIR Pr^{3+} emission (e.g. ca. 1020 nm and 1432 nm) increases under 458 nm excitation (Supplementary information Table S8). However, the observation of emission from the $^3P_1$ level, when fast relaxation to the $^3P_0$ level would be expected, and likewise emission from the $^3F_4$ and $^3F_3$ levels imply that such processes do not fully quench the emission. We note that the emission obtained from Pr(**3**)$_3$ under 458 nm excitation is very weak in comparison to that of the other complexes (Table 1). The reasons for this are unclear but may be related to the difficulties experienced in forming solutions of this complex for UV-Vis-NIR absorption studies.

The ca. 1020 nm PLE spectra of Pr(**1**-**4**)$_3$ are shown in Figure 6(a) within which the direct absorption of the Pr^{3+} ion is clearly identified. Within the UV region Pr(**1**-**3**)$_3$ also show a broader PLE peak demonstrating sensitization of the Pr^{3+} by ligand absorption. The efficiency of this process is clearly low (and of comparable strength to direct excitation of the ion) although it does increase with substitution to

form Pr(**2**)$_3$ and Pr(**3**)$_3$. It is found that sensitization of the Pr^{3+} by ligand absorption in Pr(**4**)$_3$ is weaker than that of Pr(**1**)$_3$ which is aligned with ligand emission in Pr(**4**)$_3$ providing a competing relaxation mechanism (Fig 3(c),(d)).

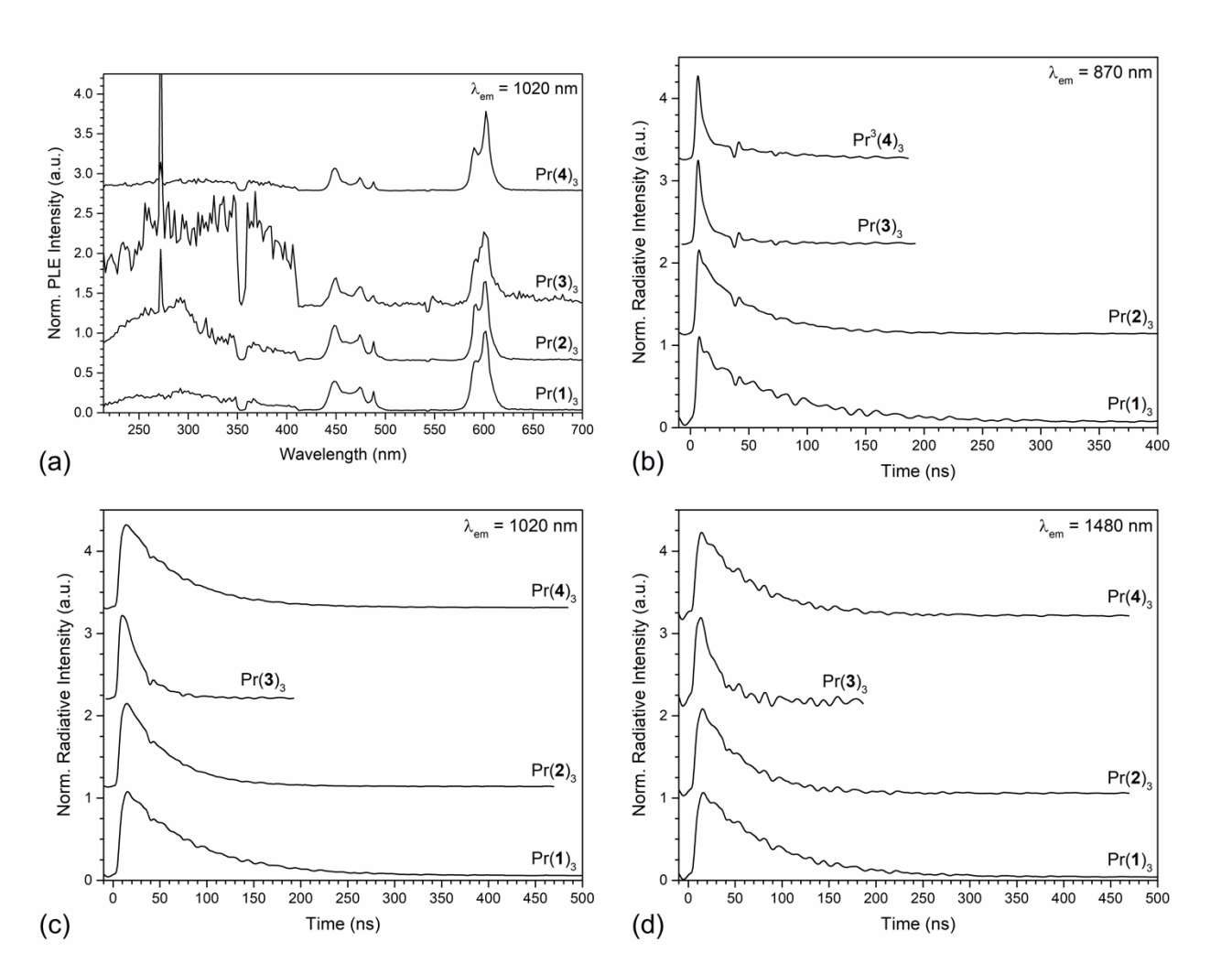

Figure 6. PLE spectra of Pr(1-4)$_3$ obtained at an emission wavelength of 1020 nm corresponding to the Pr^{3+} $^1G_4 \rightarrow {}^3H_4$ emission (a). PL decay transients of Pr(1-4)x obtained under 450 nm excitation at emission wavelengths of 870 nm (b), 1020 nm (c) and 1480 nm (d) corresponding to the Pr^{3+} $^3P_1 \rightarrow {}^1G_4$, $^1G_4 \rightarrow {}^3H_4$ and $^3F_4 \rightarrow {}^3H_4$ transitions respectively.

The 450 nm excited radiative lifetime of the Pr^{3+} $^3P_1 \rightarrow {}^1G_4$ (870 nm), $^1G_4 \rightarrow {}^3H_4$ (1020 nm) and $^3F_4 \rightarrow {}^3H_4$ (1480 nm) transitions in each complex are shown in Figures 6(b) to (d). The Pr^{3+} emission at ~610 nm was not measured due to the presence of strong ligand emission. The decay transients of Pr(**1,2**)$_3$ can

be fitted with a single exponential decay with the characteristic lifetimes shown in supplementary information Table S9. Likewise, the 1020 nm and 1480 nm decay transients of Pr(**3**,**4**)$_3$ can also be fitted with single exponential decays respectively, using the values in supplementary information Table S10. The presence of some ligand emission at ~870 nm in these complexes however requires the use of a double exponential decay to obtain a fit. The fast components of the decays are found to be 5.2 ± 0.2 ns and 4.4 ± 0.2 ns for Pr(**3**)$_3$ and Pr(**4**)$_3$ respectively, which are similar to the radiative lifetime of the ligand emission (~8 ns, supplementary information Table S6). It is generally found that the measured lifetime of the Pr^{3+} emission reduces with substitution of the 4-position of the pyridine ring in the order H > OH > Cl. Substitution of the 3,5-positions with Br, in addition to the 4-position with OH, is seen to limit the effect of the OH thus it might be expected that bromination alone could yield an increase in the Pr^{3+} emission lifetime in these complexes. PLQE measurements under 458 nm excitation (supplementary information Figure S6) reveals that in all cases the Pr^{3+} emission sensitization is poor with Pr(**1**,**2**)$_3$ having the highest efficiencies at just ~0.065% (supplementary information Table S11). A significant reduction is found when Cl is substituted at the 4-position and Br at the 3,5-positions of the pyridine ring. This correlates well with the strength of the PL spectra shown in Figure 5(b) as indicatively determined by examination of the level of noise present in each spectrum.

Using the absorption spectra in Figure 4 Judd-Ofelt modelling was performed for each complex with the exception of Pr(**3**)$_3$ because no absorption spectrum could be obtained for this complex. The measured absorption cross-sections and the measured and calculated line strengths are shown in supplementary information Table S12 for Pr(**1**)$_3$ with those of Pr(**2**,**4**)$_3$ being similar. Using this data the Judd-Oflet parameters ($\Omega_{2,4,6}$) were obtained and are shown in supplementary information Table S13. In each case an accurate least squares fit could be obtained, though the values of ΔS_{rms} are of the order 1 x 10^{-30} cm^2. It is known that Pr^{3+} often presents difficulties when attempting to utilize the Judd-Ofelt approach.[50] Thus we believe that the values obtained for ΔS_{rms} substantially overestimate the true accuracy of this fit.

3.3 Nd^{3+}-Complexes

We now present the optical characterization of Nd(**1**-**4**)$_x$ and in Figure 7(a) show the absorption spectra of each complex. Inspection of the low-energy Nd(**4**)$_1$ ligand absorption reveals similar behavior to that observed for Gd(**4**)$_2$ but without the presence of a peak at ca. 340 nm evidenced by a shoulder in the case of Pr(**4**)$_3$. On the evidence presented it is clear that the intensity and composition of the ligand absorption of the Ln(**4**)$_x$ complexes is sensitive to the molecular configuration, varying in particular over the 260 nm to 360 nm spectral range. The reduction in the ligand absorption of Nd(**4**)$_1$ is in agreement with elemental analysis supporting the Gd(**4**)$_2$ ligand coordination assignment in both cases. Taking these variations into account we still observe that the absorption of Nd(**1**-**4**)$_x$ exhibits the same shift of the absorption edge with ligand substitution discussed above for Gd(**1**-**4**)$_x$. Figure 7(b) shows the detailed absorption spectra due to the Nd^{3+} intra-atomic 4*f* transitions extending across the visible region and into the NIR spectral region. The spectra of Nd(**2**)$_3$, Nd(**3**)$_3$ and Nd(**4**)$_1$ have been offset by 12, 24 and 36 *l*$mol^{-1}cm^{-1}$ respectively for clarity. Each transition originates from the Nd^{3+} $^4I_{9/2}$ ground state to that indicated within Figure 7(b). Unlike the complexes discussed so far it can be seen that excitation at 351 nm will excite both the ligand and Nd^{3+} ($^4I_{9/2} \rightarrow {}^4D_{3/2}$) as does the 458 nm excitation ($^4I_{9/2} \rightarrow {}^4G_{11/2}$, $^2D_{3/2}$) (Figure 3).

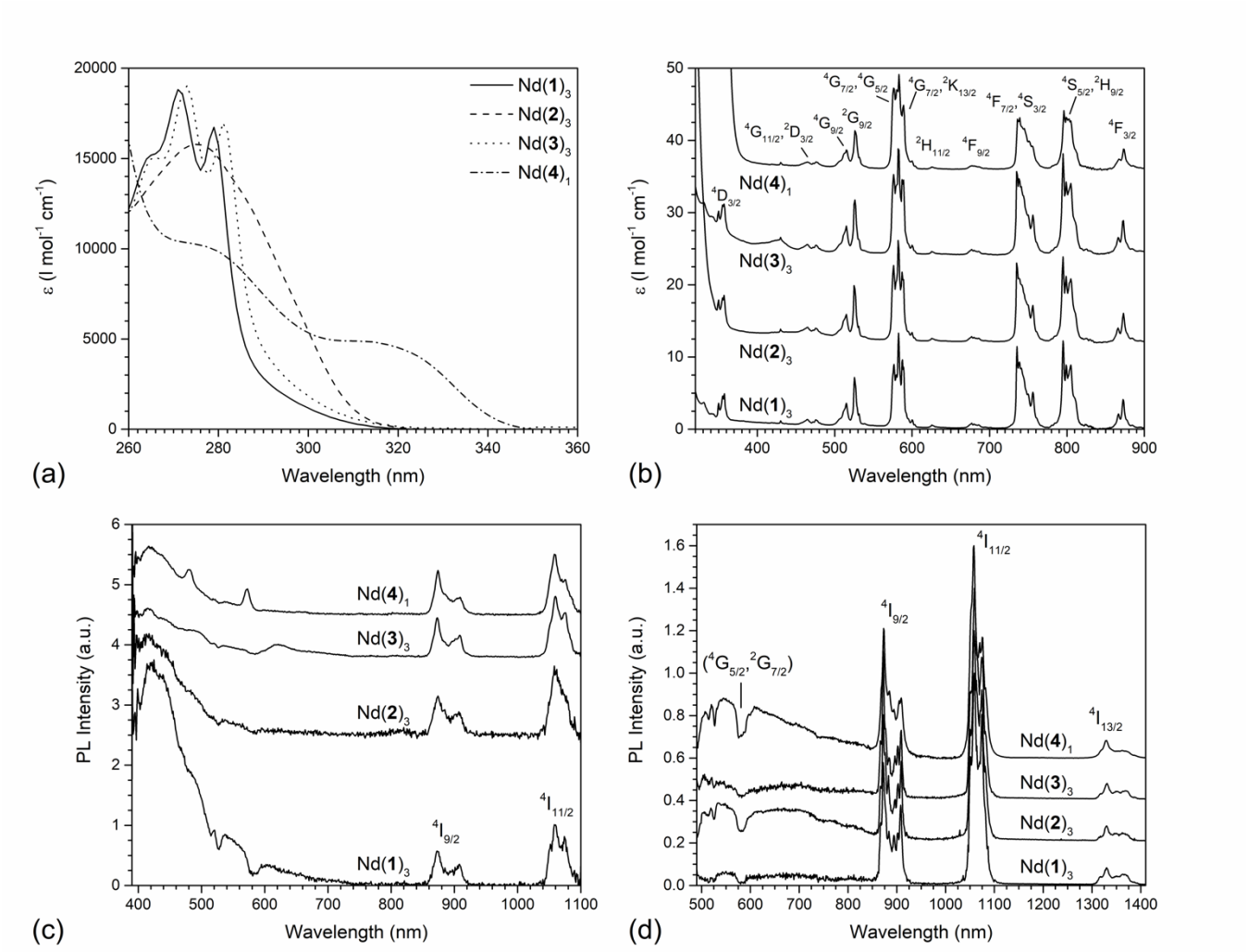

Figure 7. Absorption spectra in methanol (except Nd(**2**)$_3$ in H_2O) (a) and (b) and 351 nm and 458 nm excited powder photoluminescence spectra ((c) and (d) respectively) of neodymium(III) *tris*(pyridine-2,6-dicarboxylic acid) and its analogues [Nd(**1**-**4**)$_x$]. Nd^{3+} 4*f*-4*f* absorption transitions occur from the $^4I_{9/2}$ ground state to those indicated (using parentheses in emission spectra). 4*f*-4*f* emission occurs from the $^4F_{3/2}$ level to those indicated.

The 351 nm excited PL spectra of the Nd^{3+} complexes, each normalized to the 1053 nm emission intensity and offset for clarity, are presented in Figure 7(c). In the case of Nd(**1**)$_3$ broad ligand PL is observed peaking at 425 nm. As ligand substitution occurs the intensity of the ligand PL (in comparison to the 1053 nm PL) reduces in the order Nd(**1**)$_3$ > Nd(**2**)$_3$ > Nd(**4**)$_1$ ≈ Nd(**3**)$_3$ which also follows the relative increase in Nd^{3+} emission (Table 1). Within the low-energy tail of Nd(**1**)$_3$ ligand emission, re-absorption by Nd^{3+}

is seen, most notably at ca. 515/525 nm and ca. 584 nm corresponding to excitation of the ($^4G_{9/2}$ + $^2G_{9/2}$) and ($^2G_{7/2}$ + $^4G_{5/2}$ + $^4G_{7/2}$) levels respectively. Closer inspection also reveals excitation of the ($^4G_{11/2}$ + $^2P_{3/2}$) at ca. 476 nm. Nd(**2**-**3**)$_3$ display very similar behavior with the ligand emission being absorbed by the central ion whilst in contrast Nd(**4**)$_1$ appears to display two 'emission peaks' centered at 465 nm and 567 nm. Following detailed experimental study and careful consideration of the known Nd^{3+} 4*f* energy level structure we conclude that the 465 nm 'peak' is an artifact relating to the weak nature of the ligand emission and 'strong' absorption of the PL by the ($^4G_{11/2}$ + $^2P_{3/2}$) levels either side of this wavelength. Likewise the 'peak' at ca. 567 nm arises from a similar process involving excitation of the ($^4G_{9/2}$ + $^2G_{9/2}$) and ($^2G_{7/2}$ + $^4G_{5/2}$ + $^4G_{7/2}$) levels either side of this wavelength. Emission is observed in the NIR from Nd(**1**-**4**)$_x$ peaking at 873 nm and 1053 nm originating from the Nd^{3+} $^4F_{3/2} \rightarrow {}^4I_{9/2}$ and $^4F_{3/2} \rightarrow {}^4I_{11/2}$ transitions respectively.

To study further ligand-to-Nd^{3+} energy transfer processes the 458 nm excited PL spectra presented in Figure 7(d) may be utilized. As for the 351 nm excited PL spectra we have normalized the spectra to the 1053 nm peak intensity and offset them for clarity. It is immediately observed that we still see broad ligand PL with the similar characteristic features relating to absorption of the emission by the Nd^{3+}. The strength of the ligand PL increases as Nd(**4**)$_1$ > Nd(**2**)$_3$ > Nd(**3**)$_3$ > Nd(**1**)$_3$. The triplet energy level of Nd(**4**)$_1$ should lie between the Nd^{3+} $^4G_{7/2}$ and $^2G_{7/2}$ levels hence reduced energy transfer would be expected accounting for the ligand emission. Assuming a similar increase in triplet state energy in line with that described for Pr(**1**-**4**)$_x$ the triplet state of Nd(**1**)$_3$ would be resonant with the $^4G_{9/2}$ allowing energy transfer and the observed quenching of ligand emission. Nd(**2**-**3**)$_3$ are between these extremes resulting in the observed ligand emission behavior via interaction with the $^2G_{9/2}$ and $^4G_{7/2}$ levels.

This argument does not explain the changes in ligand emission upon 351 nm excitation as for Nd(**1**)$_3$ significant PL was observed unlike when exciting at 458 nm. This we believe is due to fast radiative recombination of the ligand singlet state competing with ISC to the triplet state. As ISC increases with

ligand substitution the triplet state is populated resulting in more efficient sensitization of the Nd^{3+} evidenced by the stronger emission (qualified by the reduction in signal noise) observed at ca. 1053 nm.

Turning attention to the emission originating from Nd^{3+} we observe 873 nm, 1053 nm, and 1330 nm centered PL due to $^4F_{3/2} \rightarrow {}^4I_{9/2}$, $^4F_{3/2} \rightarrow {}^4I_{11/2}$, and $^4F_{3/2} \rightarrow {}^4I_{13/2}$ transitions respectively. A higher resolution PL spectrum for Nd(**1**)$_3$ is provided in the supplementary information (Figure S7) revealing some of the Stark splitting detail of these levels. To obtain information regarding the relative efficiency of each transition, the peaks were each integrated and then divided by their combined sum for each complex (supplementary information Tables S14 and S15). The 1053 nm emission varies between 55% and 60% of the near infrared emission with the 873 nm and 1330 nm emission typically accounting for ca. 35% and ca. 8% respectively under 458 nm excitation. No strong correlation is observed for this excitation between the relative strengths and ligand substitution performed except for the observation that Nd(**4**)$_1$ shows the lowest proportion of 1053 nm and 1330 nm emission. This may be related to increased non-radiative relaxation of the ion due to the presence of solvent molecules that satisfy the Nd^{3+} coordination requirement in this complex. Additionally, we note that this excitation energy is able to directly excite the Nd^{3+} ($^4I_{9/2} \rightarrow {}^4G_{11/2}$) thus, whilst energy transfer from ligand to Nd^{3+} is observed to take place, direct excitation may be dominant.

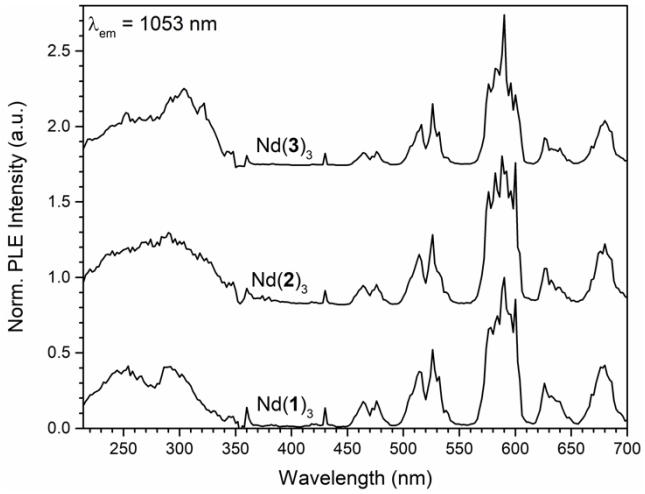

Figure 8. PLE spectra of Nd(**1**-**3**)$_3$ obtained at an emission wavelength of 1053 nm corresponding to the Nd^{3+} $^4F_{3/2} \rightarrow {}^4I_{11/2}$ emission.

PLE spectra obtained using the $^4F_{3/2} \rightarrow {}^4I_{11/2}$ (1053 nm) emission line were obtained for Nd(**1**-**3**)$_3$ and are shown in Figure 8 normalized to the absorption peak at 580nm and offset for clarity. Due to shortage of material no spectrum was obtained for Nd(**4**)$_1$. All three Nd^{3+} complexes show relatively similar PLE spectra with a broad peak in the UV region from approximately 215 nm to 350 nm. In the case of Nd(**2**)$_3$ this broad peak is centered in the middle of this PLE range at ~280 nm. In contrast the same broad peak of Nd(**1**)$_3$ appears to be a doublet peaking at ~250 nm and 295 nm with similar intensity. Finally in the case of Nd(**3**)$_3$ this broad peak appears similar in form to that of the doublet of Nd(**1**)$_3$ however the intensity of the higher energy peak at ~250 nm is significantly weaker. On comparison of the results with the ligand absorption, Figure 7(a), we can see that the strong absorption present at ~275 nm does not produce efficient photoluminescence from the complexes of Nd(**1**,**3**)$_3$. In the case of Nd(**2**)$_3$ however there is evidence that the maximum PLE intensity due to ligand absorption at ~280 nm also coincides with the peak absorption. The broad PLE peak seen in the UV region from all of the Nd^{3+} complexes suggests that energy transfer from the ligand to the Nd^{3+} ion takes place and is most efficient between 280 nm and 300 nm.

In the visible and near-IR the PLE spectra correlate with the absorption spectra presented in Figure 7(b) with peaks clearly visible due to direct intra-atomic transitions of Nd^{3+}. It can be seen that the PLE peaks attributed to the ligand absorption are in general more intense than those of direct excitation of the Nd^{3+} ion other than at ~580 nm. This suggests that ligand excitation and energy transfer into the Nd^{3+} ion can be used as a preferential sensitization mechanism.

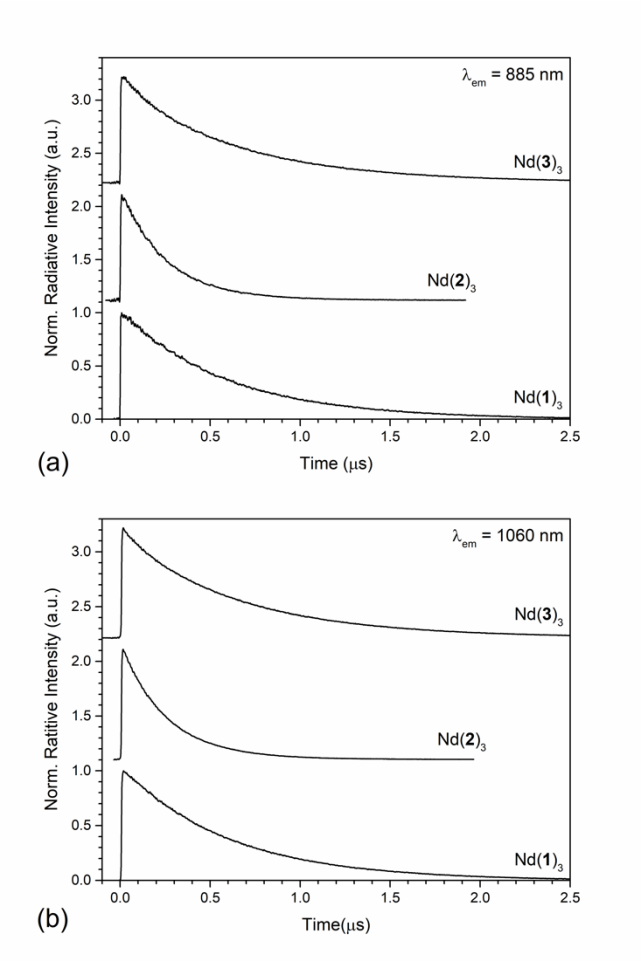

Figure 9. 520 nm excited PL decay transients of Nd(**1**-**3**)$_3$ measured at 885 nm (a) and 1060 nm (b) corresponding to the Nd^{3+} $^4F_{3/2} \rightarrow {}^4I_{9/2}$ and $^4F_{3/2} \rightarrow {}^4I_{11/2}$ transitions respectively.

Room temperature (~298 K) PL decay transients of Nd(**1**-**3**)$_3$, measured at 885 nm and 1060 nm, are presented in Figure 9(a) and (b) respectively. In both cases 520 nm excitation was used which is consistent with direct excitation of the Nd^{3+} ion and provides an indication as to how the substitution of the 3, 5 and 4 positions of the pyridine affect the non-radiative energy loss within the excited ion. It can clearly be seen that the 885 nm PL of Nd(**2**)$_3$ decays far more quickly than those of Nd(**1**,**3**)$_3$ with respective lifetimes of 248.3 ± 0.4 ns, 591.6 ± 0.4 ns and 615.8 ± 0.4 ns (supplementary information Table S16). It is therefore observed that the lifetime reduces with substitution in the order of Cl > H >> OH. where 4-Cl has the longest radiative emission. The short lifetime found for Nd(**2**)$_3$ is indicative of competing non-radiative relaxation pathways which is attributed to energy loss from the Nd^{3+} $^4F_{3/2}$ energy (~1.42 eV) level through

coupling to the (3rd harmonic) vibrational mode of O-H (~1.30 eV). The analysis of the ~1060 nm PL lifetime reveal a similar trend and lifetimes to those measured at 885 nm with values of 598.5 ± 0.3 ns, 250.4 ± 0.3 ns and 628.6 ± 0.3 ns for Nd(**1**-**3**)$_3$ respectively. This clearly supports the rationale for halogenation of the chelating ligands in order to reduce deleterious non-radiative relaxation.

The PLQE of the Nd^{3+} emission for Nd(**1**-**3**)$_3$, when excited at 514 nm, is given in supplementary information Table S17 calculated using the spectra shown in supplementary information Figure S8. As expected from the PL lifetime data the PLQE reduces with substitution of the 4-postion with OH and is increased when substituted with Cl. It is interesting to note that in the case of Nd(**4**)$_1$ the PL intensity of the Nd^{3+} emission at ~885 nm and 1060 nm appears almost as strong as that of Nd(**3**)$_3$ (Figure 7(c)). In this case, although lack of material prevented our measurement of the lifetime and PLQE, the substitution of the 3,5-position of the pyridine ring with Br must be balancing the potentially deleterious effect of the OH group present at the 4-position (and indeed any solvent molecules completing the coordination).

The Judd-Ofelt phenomenological parameters for Nd(**1**-**4**)$_x$ were calculated from the measured and calculated oscillator strengths and are presented in supplementary information Table S18 and S19. It can be seen that a good least squares fit was achieved for all parameters with the largest root mean square oscillator strength error (ΔS_{rms}) being found for Nd(**4**)$_1$, with a value of 0.66 x10^{-20} cm^2. These values compare well with those obtained by a study of lead-doped silicate glass[51] and $GdAl_3(BO_3)_4$ crystal[52] hosts. Using these values the calculated branching ratios (supplementary information Table S20) of the complexes were obtained for each complex along with their calculated radiative lifetimes and efficiencies. These are presented in supplementary information Table S21 alongside the experimentally measured radiative lifetimes. As the Judd-Ofelt theory does not account for any non-radiative energy loss the lifetimes calculated (τ_{calc}) are typically far longer (~ three orders of magnitude) than those of the experimentally measured lifetimes (τ_{meas}). Although a direct comparison of the calculated and measured radiative lifetimes cannot be made, the order of the radiative lifetimes between the complexes is still of interest. As previously discussed the experimentally measured radiative lifetimes of the Nd(**1**-**3**)$_3$

complexes take the order 4-Cl > dpa >> chel where 4-Cl has the longest radiative emission. In the case of the radiative lifetimes calculated using Judd-Ofelt theory, the Nd^{3+} complexes take the order dpa >> chel > 4-Cl. The most notable difference here is that the Nd(**3**)$_3$ has the shortest calculated radiative lifetime and the longest measured radiative lifetime. As the Judd-Ofelt theory does not account for the effects of non-radiative loss this is further evidence that halogenation of the complex specifically reduces the non-radiative relaxation thereby increasing the measured radiative lifetime. Furthermore, comparison of the PLQE obtained from the Judd-Ofelt model to those obtained experimentally again shows an over-estimate (by ~four orders of magnitude) of the PLQE by the model (supplementary information Table S21). Recalling the experimentally measured PLQE, for Nd^{3+} they take the order 4-Cl > dpa >> chel whilst in contrast the Judd-Ofelt calculated QE reveal that the trend 4-Cl >> chel > dpa.

3.4 Dy^{3+}-Complexes

As for the above complexes we present similar optical spectra in Figure 10 for Dy(**1**-**4**)$_x$. The ligand absorption spectra (Figure 10(a)) are most similar to that of Gd(**1**-**4**)$_x$ with the only significant difference being the reduction in the molar extinction coefficient of Dy(**3**)$_1$ by two thirds. We believe that this is directly related to the reduction in ligand coordination to the Dy^{3+} which in contrast to all other complexes of (**3**) did not fully coordinate the ion, as confirmed by ScXRD. Again the ligand absorption of Dy(**4**)$_3$ agrees with elemental analysis, increasing to a level similar to the other 3-ligated complexes.

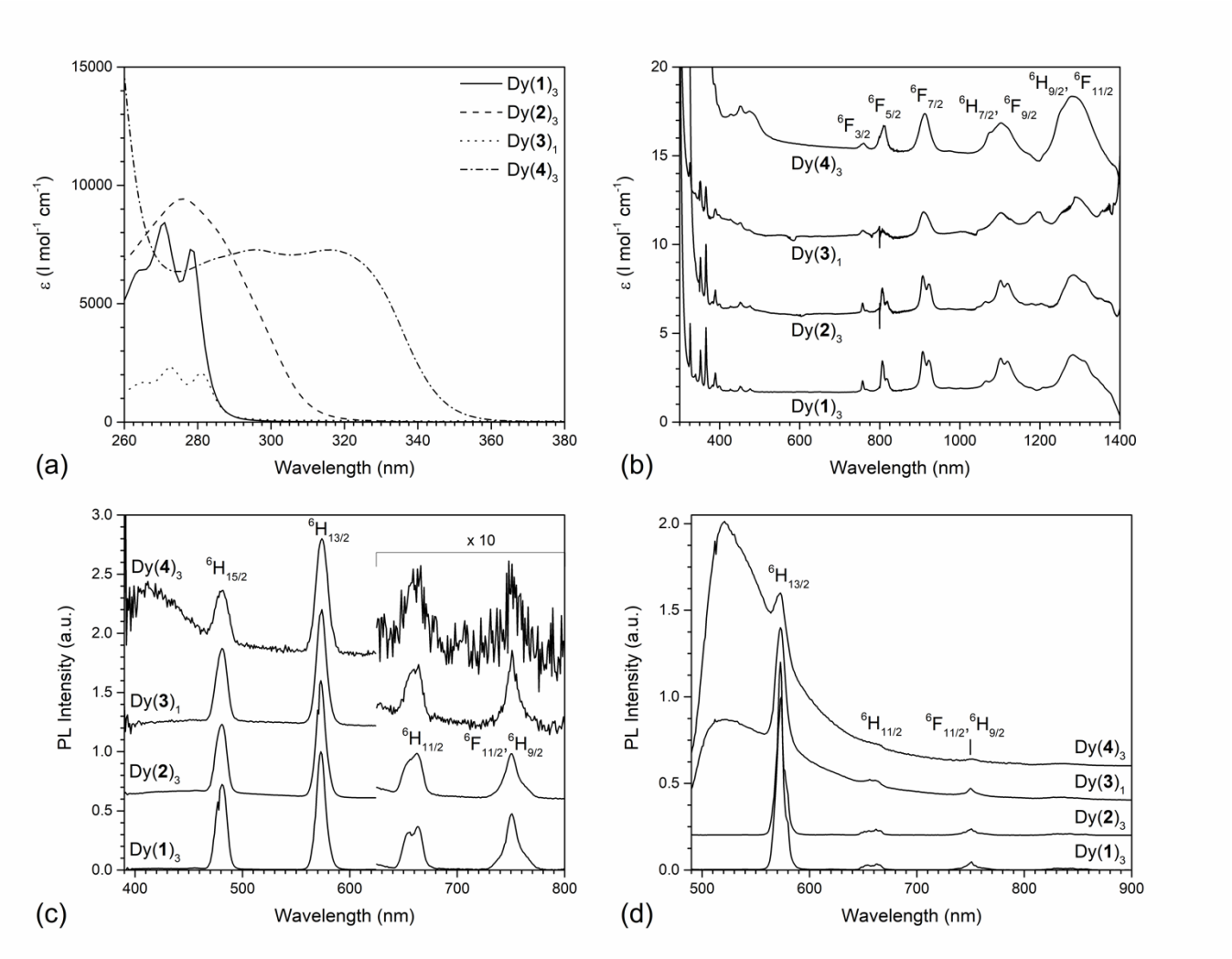

Figure 10. Absorption spectra in methanol (a) and (b) and 351 nm and 458 nm excited powder photoluminescence spectra (c) and (d) respectively, of dysprosium(III) *tris*(pyridine-2,6-dicarboxylic acid) and its analogues [Dy(**1**-**4**)$_x$]. Dy^{3+} 4*f*-4*f* absorption transitions occur from the $^6H_{15/2}$ ground state to those indicated. 4*f*-4*f* emission occurs from the $^4F_{9/2}$ level to those indicated.

The 4*f* Dy^{3+} absorption of each complex is shown in Figure 10(b) extending out to 1400 nm with all transitions occurring from the $^6H_{15/2}$ ground level to those indicated. Many transitions in the 300 nm to 500 nm spectral region are observed, and are particularly clear for Dy(**1**)$_3$ which are shown in more detail in supplementary information Figure S9(a). At energies above 400 nm (3.1 eV, 25000 cm^{-1}) definitive assignment of the energy levels becomes complex due to intense overlap and mixing of the *J* states. Various attempts have been made in early work[40,41] and based on more recent studies,[53-56] however

variation in assignment still exists. Our assignments in this region are based on consideration of these previous reports.

The $^6H_{15/2} \rightarrow {}^6F_{11/2}$ transition has previously been reported[57-59] to be hypersensitive to the local atomic configuration observed via changes in the relative contribution to the absorption at ca. 1300 nm due to this transition and the $^6H_{15/2} \rightarrow {}^6H_{9/2}$ transition. However, despite the change in ligand coordination between Dy(**1**,**2**,**4**)$_3$ and Dy(**3**)$_1$ no quantifiable change could be observed in the absorption spectrum beyond the slight reduction in the high energy side of this absorption in the case of Dy(**3**)$_1$.

It can be observed that excitation at 351 nm results in both ligand and Dy^{3+} excitation (via the $^6H_{15/2} \rightarrow {}^6P_{5/2}$ transition). The 458 nm excitation is however only very weakly absorbed by the Dy^{3+} via the $^6H_{15/2} \rightarrow {}^4I_{15/2}$ transition (supplementary information Figure S9(a) and Figure 3). The PL resulting from 351 nm excitation, shown in Figure 10(c), reveals four emission bands originating from the Dy^{3+} $^4F_{9/2}$ level populated via non-radiative relaxation from the $^6P_{5/2}$ level pumped by the excitation energy. We have normalized the spectra to the Dy^{3+} ca. 574 nm emission and offset the spectrum of Dy(**2**-**4**)$_x$ for clarity. Only Dy(**4**)$_3$ displays any significant ligand emission (much weaker emission is observable from Dy(**3**)$_1$) thus following excitation of the ligand singlet state of Dy(**1**-**3**)$_x$ it is able to relax via efficient energy transfer to the Dy^{3+} (via the $^4I_{13/2}$, $^4F_{7/2}$ levels). Figure 3 shows that in the case of Dy(**4**)$_3$ the singlet ligand state is not resonant with a 4*f* intra-atomic level of Dy^{3+} being below the $^4G_{11/2}$ level.

The four PL peaks originating from the Dy^{3+} are all related to the relaxation of the $^4F_{9/2}$ level with the 481 nm ($^4F_{9/2} \rightarrow {}^6H_{15/2}$) and 574 nm ($^4F_{9/2} \rightarrow {}^6H_{13/2}$) being the strongest and the former decreasing and latter increasing in relative intensity upon ligand substitution (supplementary information Table S22). The 664 nm ($^4F_{9/2} \rightarrow {}^6H_{11/2}$) peak also increases with ligand substitution whilst the 750 nm ($^4F_{9/2} \rightarrow {}^6H_{9/2}$, $^6F_{11/2}$) PL remain at constant relative intensity in each complex. However, as can be seen by the increase in spectral noise the overall PL yield reduces as the ligands are modified in the order Dy(**1**)$_3$ ≈ Dy(**2**)$_3$ > Dy(**3**)$_1$ > Dy(**4**)$_3$ (Table 1). The significant reduction in overall PL yield from the Dy^{3+} in the case of Dy(**4**)$_3$ has been discussed above and is attributed to reduced ligand to Dy^{3+} energy transfer thus reducing

sensitization via this route. The noticeable reduction in Dy(**3**)$_1$ may again be due to the reduced energy transfer compared to Dy(**1**-**2**)$_3$ as evidenced by the small amount of ligand emission still observable. No lower energy PL emission from the Dy^{3+} was measured from any of the complexes under 351 nm excitation.

Excitation at 458 nm directly excites the Dy^{3+} $^4I_{15/2}$ level in addition to the ligands. The excited $^4I_{15/2}$ energy level should undergo fast non-radiative relaxation to the $^4F_{9/2}$ energy level, although as we have shown above such a process in Pr(**1**-**4**)$_x$ was not completely dominant. Having excited the $^4F_{9/2}$ level it would be expected that very similar Dy^{3+} emission would be observed from Dy(**1**-**4**)$_x$ under either excitation wavelength (351 nm or 458 nm). Inspection of the PL spectra obtained under 458 nm excitation (again normalized to the ca. 574 nm emission and offset for clarity) reveal remarkable differences in contrast to this expectation, Figure 10(d). We firstly note that the use of long-pass filters to remove scattered 458 nm excitation also precludes observation of the 481 nm Dy^{3+} emission. Secondly, strong ligand emission is now observed centered at ca. 520 nm from Dy(**3**-**4**)$_x$ with no ligand emission observed from Dy(**1**-**2**)$_3$. This is immediately explained by inspection of Figure 3 and the relative position of the complex triplet state energy which for Dy(**4**)$_3$ lies below the Dy^{3+} $^4F_{9/2}$ energy level preventing energy transfer. For Dy(**1**-**2**)$_3$ energy transfer may occur from the triplet state as its energy increases, as discussed above for these complexes, into the $^4F_{9/2}$ level hence quenching the ligand emission. Comparison of the ligand emission obtained under 351 and 458 nm excitation indicates that energy transfer must also occur directly from the singlet state. If this were not the case, stronger emission would be expected under 351 nm excitation following ISC to the triplet state. We may therefore also therefore assume that the lack of ligand emission from the other complexes under 351 nm excitation is due to a similar process rather than via ISC to the triplet state and subsequent energy transfer. This former energy transfer route is likely to be more efficient being based on a Dexter process ($|\Delta J| = 1$) with transfer into the $^4F_{9/2}$ being much weaker ($|\Delta J| = 3$).

Closer inspection of the 458 nm excited PL in Figure 10(d) indicates the presence of a further peak at ca. 850 nm in the spectra. We show in supplementary information Figure S9(b) a detailed PL spectrum of Dy(**1**)$_3$ over an extended spectral region that reveals many more peaks resulting from Dy^{3+} intra-atomic transitions. Radiative emission is observed originating from the $^4F_{9/2}$ level to every lower lying level, as assigned within Figure S9(b), with the longest such transition being observed at ca. 1287 nm due to the $^4F_{9/2} \rightarrow {}^6F_{1/2}$ transition as a doublet. We also observe this transition in Dy(**2**-**3**)$_x$ but only extremely weakly in Dy(**4**)$_3$ (supplementary information Figure S9(c) and Table S23). In Dy(**1**)$_3$ the observation of a lower energy transition at ca. 1350 nm ,which we assign to the ($^6F_{11/2}$, $^6H_{9/2}$) $\rightarrow {}^6H_{15/2}$ transition, and a very weak emission at ca. 1855 nm assigned to the $^6H_{11/2} \rightarrow {}^6H_{15/2}$ transition is seen (supplementary information Figure S9(d)). We note that this emission, which is the longest reported from such a complex, is at the limits of the system detection range used and hence (despite correction for the system response) may be more intense than indicated in supplementary information Figure S9(d). Of the other complexes studied only Dy(**3**)$_1$ demonstrated (much weaker) emission at ca. 1350 nm and no other complexes exhibited any detectable emission at 1855 nm. As such no further information on any potential hypersensitivity of the $^6F_{11/2} \rightarrow {}^6H_{15/2}$ could be gained as previously reported[60] using these complexes alone.

Figure 11(a) presents the PLE spectra of Dy(**1**-**4**)$_x$ measured at 574 nm ($^4F_{9/2} \rightarrow {}^6H_{13/2}$), normalized to the PLE peak at 450 nm and offset for clarity. All four complexes show similar PLE spectra to those observed for the Nd(**1**-**3**)$_3$, with a broad UV peak from approximately 214 nm to 325 nm. This correlates well with the hypothesis that the broad PLE peak in the UV region is due to ligand sensitized emission of the lanthanide ion. In the case of Dy(**1**)$_3$ and Dy(**3**)$_1$ this broad peak can be seen to comprise of two overlapping bands peaking at ~250 nm and 300 nm closely mirroring, through slightly shifted, the absorption spectrum of these samples. The PLE of Dy(**4**)$_3$ shows a much sharper absorption peak at ~295 nm suggesting the existence of an intra-atomic transition at this wavelength. A low intensity broad PLE peak from approximately 215 nm to 350 nm is also observed for Dy(**4**)$_3$ suggesting that ligand sensitization is comparable to direct sensitization of the Dy^{3+} ion in this complex. The red-shift of this

peak, compared to that of the other Dy(**1**-**3**)$_x$, correlates well with the absorption data presented in Figure 10(a).

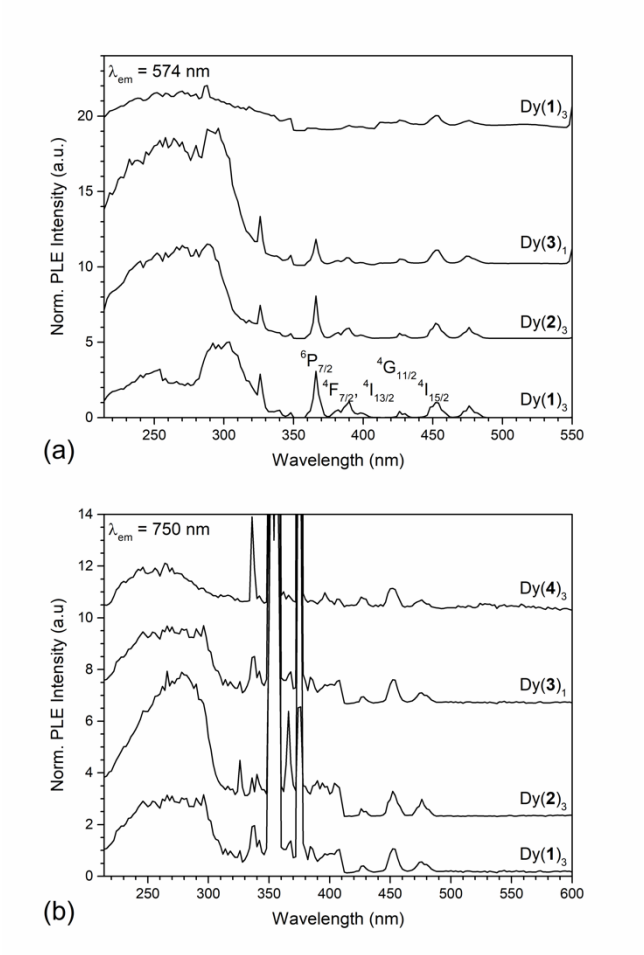

Figure 11. PLE spectra of Dy(**1**-**4**)$_x$ obtained at an emission wavelength of 574 nm (a) and 750 nm (b) corresponding to the Dy^{3+} $^4F_{9/2} \rightarrow {}^6H_{13/2}$ and $^4F_{9/2} \rightarrow {}^6H_{9/2}$, $^6F_{11/2}$ transitions respectively.

It should be noted that as the PLE was obtained at 574 nm it is possible that ligand-centered emission in addition to Dy^{3+} centered emission was being detected. (c.f. Figure 10(c) and (d) where under 351 nm and 458 nm excitation Dy(**4**)$_3$ exhibited strong emission attributed to the ligand at 574 nm). Figure 11(b) therefore presents additional PLE spectra measured at 750 nm to prevent such a possibility, as negligible ligand emission is observed at this wavelength. In the visible region the PLE spectra correlate well with the absorption spectra of Dy(**1**-**4**)$_x$ with peaks at ~326 nm, ~366 nm, ~389 nm, ~428 nm, ~452 nm and ~476 nm matching the Dy^{3+} intra-atomic transitions. The 750 nm PLE displays a narrower broad peak in

the UV region at ~295 nm for the Dy(**1**)$_3$ and Dy(**3**)$_1$ and no sharp peak at 295 nm for Dy(**4**)$_3$ when compared to the 574 nm PLE. Additionally, very intense PLE peaks at approximately 355 nm and 375 nm are now observed for all complexes, attributed to the $^6H_{15/2} \rightarrow {}^6P_{5/2}$ and $^6H_{15/2} \rightarrow {}^6P_{7/2}$ intra-atomic transitions respectively (supplementary information Figure 9(a)). The lack of the distinct UV PLE peaks in Figure 11(b) could indicate that those observed in Figure 11(a) could be due to ligand-centered emission rather than Dy^{3+} sensitized emission as the excitation wavelength of 295 nm matches the predicted energy level for the triplet state for the Gd(**4**)$_2$ ligand.

Within the 750 nm PLE for Dy(**1**-**4**)$_x$ a strong peak is observed at 336nm due to the transition $^6H_{15/2} \rightarrow {}^4F_{5/2}$. This is in contrast to the absorption spectra where weak direct absorption is seen at this wavelength. Interestingly, this PLE peak at 336 nm is particularly strong in Dy(**4**)$_3$ and weak in Dy(**2**)$_3$, which instead has a peak at ~326 nm that is absent in the other complexes.

The relative intensities of the PLE peaks attributed to ligand-sensitized emission and direct excitation of the Dy^{3+} ion provide an indication of the PL efficiency with Dy(**4**)$_3$ appearing to have the lowest sensitization efficiency. Similar analysis leads to the expectation that the sensitization efficiency decreases in the order of chel > dpa > 4-Cl > 3,5-Br which should be observable in the PL lifetime. The 574 nm ($^4F_{9/2} \rightarrow {}^6H_{13/2}$) PL transient decays are shown in Figure 12 and found to be biexponential in nature with the values provided in supplementary information Table S24. The excitation wavelength used was 520 nm thus direct excitation of the Dy^{3+} ion is performed and the lifetimes obtained therefore again give an indication to the non-radiative energy losses within the ion with respect to the 4- and 3,5-position substitutions of the ligand. It is apparent that there are extreme differences in radiative lifetime of the different Dy^{3+} complexes as the longer of the biexponential lifetimes vary by two orders of magnitude from 42.83 ± 0.01μs for Dy(**1**)$_3$ to 0.61 ± 0.01 μs for Dy(**4**)$_3$. The PL lifetimes take the order dpa > chel > 4-Cl > 3,5-Br which is similar to that expected qualitatively from the PLE. The shortened lifetimes of Dy(**3**)$_1$ and Dy(**4**)$_3$ suggest an extremely inefficient radiative process and are in stark contrast to the Nd^{3+} complexes where halogenation in the case of Nd(**3**)$_3$ reduced non-radiative loss.

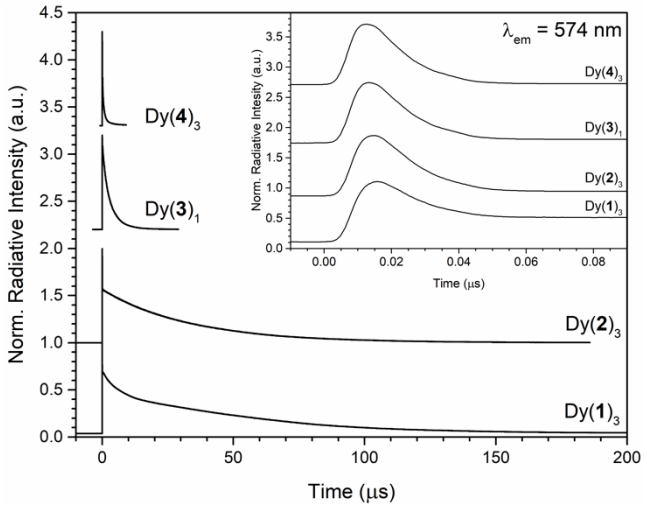

Figure 12. 520 nm excited PL decay transients of Dy(**1**-**4**)$_x$ measured at 547 nm corresponding to the Dy^{3+} $^4F_{9/2} \rightarrow {}^6H_{13/2}$ transition.

The faster of the biexponential lifetimes observed in each Dy^{3+} complex occur on a ~10 ns timescale. Due to the short duration of this component, and its unchanging nature across the four complexes, the 'fast' component is attributed to ligand-centered luminescence. This is in agreement with the study of Gd(**1**-**4**)$_x$ described above where the proposed strong **L**.**S** coupling is consistent with a bi-exponential decay being observed due to fast radiative recombination of the triplet state (Table S6).

Consideration of the results of the PLE and the PL lifetimes enables prediction of the relative PL efficiency of the Dy(**1**-**4**)$_x$. For example Dy(**4**)$_3$ displays the least intense ligand PLE and also presented the shortest radiative lifetimes, we therefore predict that it will be the least efficient of the complexes studied. Based on such argument we predict the PLQE to take the order dpa ≈ chel > 4-Cl > 3,5-Br. PLQE measurements (exciting at 458 nm) were undertaken and are presented in supplementary information Figure S10 and tabulated in supplementary information Table S25. A similar order of relative efficiency to that predicted above is observed Dy(**1**)$_3$ and Dy(**2**)$_3$ having the highest efficiencies followed by the halogenated complexes.

Judd-Ofelt theory was again employed to analyze the absorption of the complexes and used to determine their oscillator strengths, emission probabilities and branching ratios. Nine Dy^{3+} transitions were used in

the analysis of all the complexes with the exception of Dy(**4**)$_3$ where only five transitions could be used due to intense ligand absorption masking the lanthanide transitions. Supplementary information Table S26 presents the absorption cross-sections with associated oscillator strengths, measured and calculated, for each intra-atomic transition of Dy(**1**)$_3$. The Judd-Ofelt parameters obtained for each complex are presented in supplementary information Table S27 along with ΔS_{rms}. The ΔS_{rms} values suggests that the least squares fit is relatively good for all of the complexes with the highest deviation being calculated for the Dy(**1**)$_3$ at a value of 0.228 x 10^{-20} cm^2. Although ΔS_{rms} suggests a good fit for the Judd-Ofelt theory, there seems to be a large variation in the values obtained, with Ω_2 ranging from 0.66 to 7.18 (x 10^{-20} cm^2) between Dy(**2**)$_3$ and Dy(**4**)$_3$. The large discrepancy in the Ω_λ values can be attributed to the uncertainties in accurately measuring the weak absorption bands as reported by others.[61] In particular, as noted above, for Dy(**4**)$_3$ the weaker transitions were not used in the Judd-Ofelt calculation due to the intense ligand absorption as can be seen in Figure 10.

Supplementary information Table S28 presents the lifetimes for the intra-atomic transitions originating from the $^4F_{9/2}$ energy level of the Dy^{3+} complexes as calculated by the Judd-Ofelt theory. It is found as expected, discussed above, that the lifetimes predicted by the Judd-Ofelt theory are several orders of magnitude longer than those measured experimentally. Judd-Ofelt theory predicts that the lifetimes should take the order 4-Cl > chel > dpa > 3,5-Br where Dy(**3**)$_1$ has the longest lifetime in contrast to the measured lifetimes which take the order dpa > chel > 4-Cl > 3,5-Br where Dy(**1**)$_3$ has the longest lifetime. Supplementary information Table S25 presents the calculated Judd-Ofelt PLQE alongside the experimental values. In general the predictions can be seen to qualitatively agree with measurement with Dy(**1**,**2**)$_3$ having higher PLQE than Dy(**3**,**4**)$_x$.

3.5 Er^{3+}-Complexes

We finally present the optical characterization of Er(**1**-**4**)$_3$ in Figure 13. The ligand absorption is similar to that reported above for the other complexes within with that of Er(**4**)$_3$ most closely resembling that of Pr(**4**)$_3$ exhibiting a clear shoulder at ca. 340 nm and extended absorption to 360 nm (Figure 13(a)). The absorption spectrum of Er(**3**)$_3$ shows signs of background scattering of light, though the solution was observed to be fully dissolved and clear to the eye not displaying any color or turbidity. The $^4I_{15/2}$ ground state Er^{3+} 4*f* absorption is shown in Figure 13(b) with the spectrum of Er(**2**-**4**)$_3$ offset by 6, 12 and 16 *l*mol^{-1}cm^{-1} for clarity. The 690 nm to 950 nm spectral region is also excluded again to improve clarity but provided in supplementary information Figure S11(b). All complexes exhibit very similar ground state absorption with the main difference being a significant increase in the $^4I_{15/2} \rightarrow {}^2H_{11/2}$ transition with a corresponding increase in the $^4I_{15/2} \rightarrow {}^4G_{11/2}$ transition in Er(**3**)$_3$. Both of these transitions have been reported as being hypersensitive[62] which explain these observations and will be discussed further below.

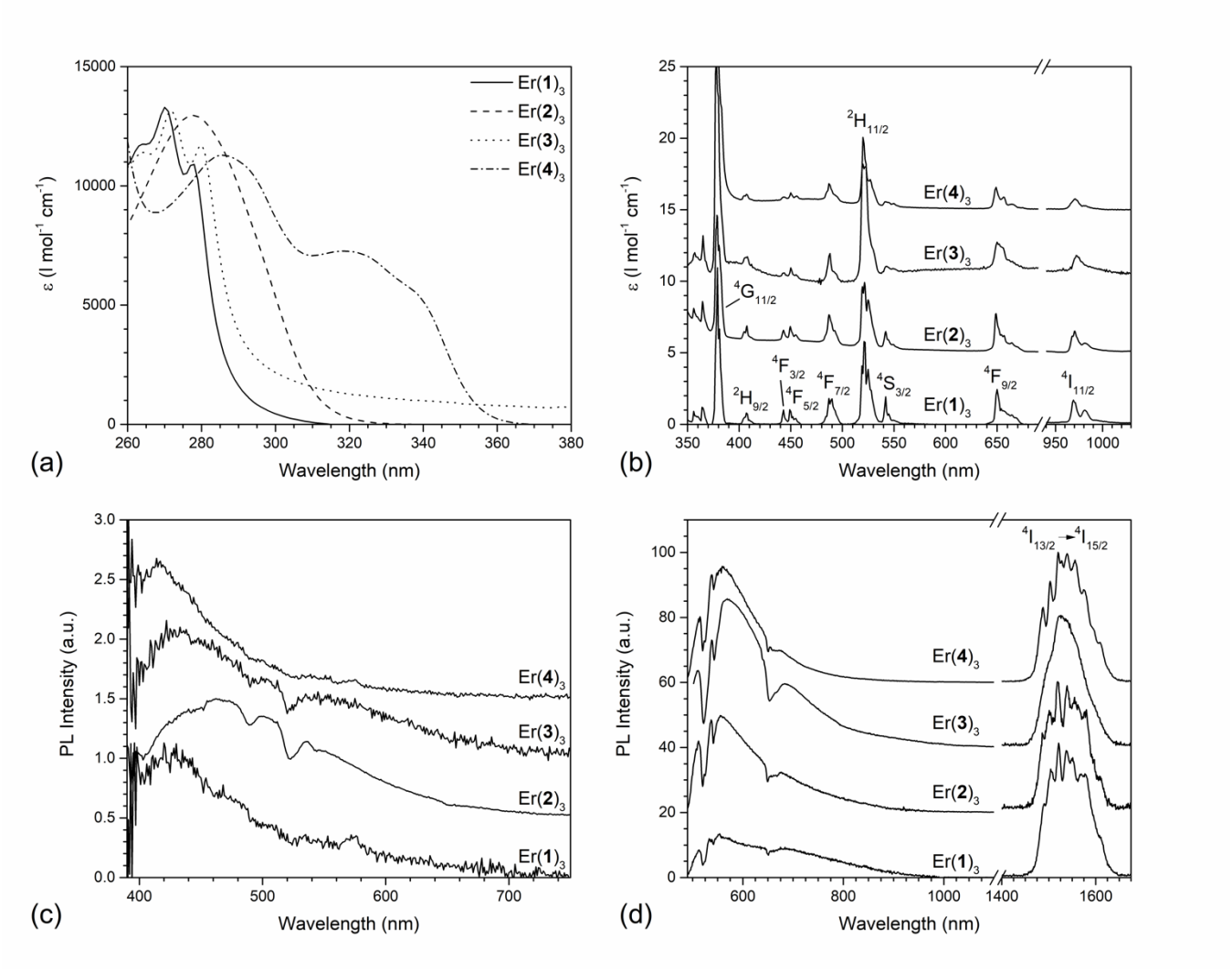

Figure 13. Absorption spectra in DMSO (except Er(**2**)$_3$ in H_2O) (a) and (b) and 351 nm and 458 nm excited powder photoluminescence spectra ((c) and (d) respectively) of erbium(III) *tris*(pyridine-2,6-dicarboxylic acid) and its analogues [Er(**1**-**4**)$_3$]. Er^{3+} 4*f*-4*f* absorption transitions occur from the $^4I_{15/2}$ ground state to those indicated. 4*f*-4*f* emission occurs due to transitions between the levels indicated.

Supplementary information Figure S11(a) and S11(b) shows the absorption of Er(**1**)$_3$ in greater detail with absorption from the $^4I_{15/2}$ level observable to every above lying level up to $^2G_{7/2}$ at ca. 356 nm. This includes very weak absorption due to the $^4I_{15/2} \rightarrow {}^4I_{9/2}$ transition at ca. 798 nm not shown in Figure 13(b). We also note that excitation at 351 nm excites only the ligand whilst 458 nm excitation mainly excites the ligand and the low-energy shoulder of the $^4F_{5/2}$ Er^{3+} energy level (supplementary information Figure S11(a) and Figure 3).

Upon excitation at 351 nm each ligand displays PL with that of Er(**2**)$_3$ being significantly stronger than the others peaking at ca. 460 nm as observed for Gd(**2**)$_3$. Within the low energy tail of Er(**2**)$_3$ (and Er(**3**)$_3$) absorption of the ligand PL by the Er^{3+} is seen at ca. 487 nm ($^4I_{15/2} \rightarrow {}^4F_{7/2}$) and 420 nm ($^4I_{15/2} \rightarrow {}^2H_{11/2}$). A smaller absorption at ca. 450 nm is also apparent due to the $^4I_{15/2} \rightarrow {}^4F_{5/2}$ transition. The weak nature of the ligand emission (compared to other Ln^{3+} complexes above) indicates quenching of the ligand singlet emission either via energy transfer to the Er^{3+} as discussed further below. Despite the direct excitation of the Er^{3+} at 351 nm (via $^2G_{7/2}$), ligand to Er^{3+} energy transfer, and absorption of ligand PL only Er(**2**)$_3$ exhibits characteristic NIR Er^{3+} emission due to the well-known $^4I_{13/2} \rightarrow {}^4I_{15/2}$ transition (supplementary information Figure S11(c)). This suggests that non-radiative intra-atomic quenching is occurring in Er(**1**,**3**-**4**)$_3$ but is less effective in Er(**2**)$_3$ (which counter intuitively has an OH group attached to the ligand) or that another process is leading to relaxation of the excited Er^{3+}.

The singlet state of Er(**4**)$_3$ will lie close to (but not quite match) the Er^{3+} $^4F_{3/2}$ level thus enabling energy transfer ($|\Delta J| = 6$) and reducing the ligand emission although not fully quenching it (Figure 3). Likewise for Er(**1**,**3**)$_3$ which lie close to the $^2H_{9/2}$ level though with $|\Delta J| = 3$ transfer is in principle likely to be less efficient than via the $^4F_{3/2}$ level. The singlet state of Er(**2**)$_3$ will lie between these Er^{3+} energy levels and therefore may account for the increased ligand emission if direct transfer from the singlet state is an important factor. Supporting this is the reduced ISC to the triplet state in Er(**2**)$_3$ (compared with Er(**3**,**4**)$_3$) because if this did occur then energy transfer from the triplet state to the Er^{3+} would quench the ligand emission as discussed below.

Inspection of the 458 nm excited PL in Figure 13(d) reveals that each complex is indeed able to exhibit strong characteristic Er^{3+} emission at ca. 1530 nm due to the $^4I_{13/2} \rightarrow {}^4I_{15/2}$ transition which is in contrast to the behavior observed under 351 nm excitation. The full spectral region excluding the break is shown in supplementary information Figure S11(d). A possible explanation is that Er^{3+} to ligand energy back-transfer may occur upon 351 nm excitation into the ligand triplet state thus preventing Er^{3+} emission in some complexes. For example Figure 3 shows that the triplet state of Er(**4**)$_3$ is likely to lie just below the

$^2H_{11/2}$ level facilitating this ($|\Delta J| = 2$). However, in such a case one might then expect triplet to Er^{3+} transfer via the $^4S_{3/2}$ energy level ($|\Delta J| = 6$) to re-sensitize the Er^{3+}, albeit with reduced efficiency. A similar argument is however difficult to make for the other Er^{3+} complexes that is consistent with the energy of the triplet states inferred from the study of the other Ln^{3+} complexes. It is therefore most likely that the ca. 1530 nm emission obtained under 458 nm excitation is mainly due to direct excitation of the Er^{3+}.

Inspection of the ligand emission obtained under 458 nm excitation shows each complex displaying significant emission with Er(**3**)$_3$ being the strongest followed by Er(**4**)$_3$, Er(**2**)$_3$ and Er(**1**)$_3$. This indicates that energy transfer from the triplet state into the Er^{3+} is only significant in the case of Er(**1**)$_3$ via the $^4F_{7/2}$ level. If this were the case then triplet-Er^{3+} energy transfer should also be observed from the other complexes, in particular into the $^2H_{11/2}$ level, though this is not strongly supported by the available data.

Figure 14(a) presents the PLE spectra of Er(**1**-**4**)$_x$ measured using the $^4I_{13/2} \rightarrow {}^4I_{15/2}$ PL at 1520 nm. Each spectrum is normalized to the PLE peak at 650 nm and offset for clarity. The loss of intensity between 350 nm and 360 nm for all the complexes is again attributed to the low excitation power available in this region. Er(**1**)$_3$ presents a PLE peak in the ultra-violet region at ~300 nm that is consistent with the PLE spectra of Nd(**1**)$_3$ and Dy(**1**)$_3$ (Figure 8 and Figure 11), however in comparison the intensity is significantly reduced. Er(**2**)$_3$ shows a slightly stronger broad peak in the UV region with a PLE edge at 300 nm. It was observed above that upon excitation at 351 nm only Er(**3**)$_3$ displayed the 1520 nm $^4I_{13/2} \rightarrow {}^4I_{15/2}$ characteristic emission. This correlates well with the PLE peak seen for this complex at approximately 350 nm and which is absent for the remaining complexes. Although there is a gap in the available wavelength range between 350 nm and 360 nm for PLE studies, extrapolation of the data either side of this wavelength range shows that excitation here should yield the most efficient sensitization for Er(**3**)$_3$. Generally for the remaining complexes however, the PLE peaks in the UV region are typically lower in magnitude than the PLE peaks in the visible region. This indicates that the Er^{3+} complexes possess a low energy transfer efficiency from the ligand to the Er^{3+} ion. The excessive noise in the broad UV PLE peak for Er(**3**)$_3$ is attributed to the effects of fluctuations in the Q-switch laser power coupled with a highly

sensitive energy transfer process. The PLE peaks in the visible region for all the Er^{3+} complexes correlate well with the intra-atomic transitions of the Er^{3+} ion seen in the absorption spectra (Figure 13(b) and supplementary information Figure S11(a) and (b)).

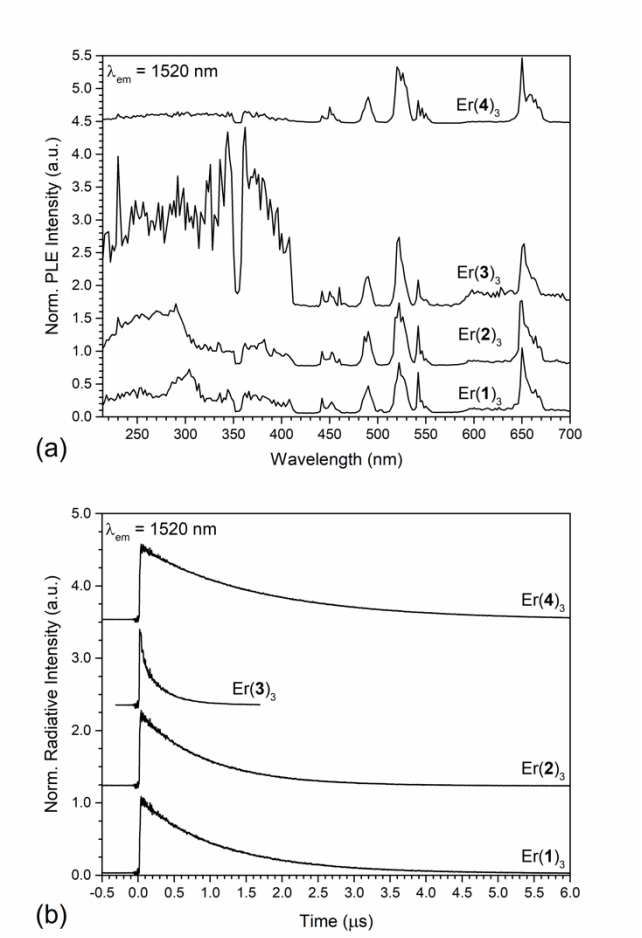

Figure 14. The PLE spectra (a) and 520 nm excited PL decay transients (b) of Er(**1**-**4**)$_3$ measured at 1520 nm corresponding to the Er^{3+} $^4I_{13/2} \rightarrow {}^4I_{15/2}$ transition.

The 520 nm excited PL decay transients of Er(**1**-**4**)$_3$ measured at 1520 nm (0.82 eV) are presented in Figure 14(b). The excitation used directly excites the Er^{3+} ion (as verified from the PLE spectra, Figure 14(a)) again enabling the lifetimes obtained to give an indication on the level of non-radiative energy losses taking place within the Er^{3+} ion. The decay transients have been normalized to their maximum intensity and all were found to display single exponential decay behavior. It is seen that Er(**3**)$_3$ has the shortest radiative lifetime and was calculated to be 0.210 ± 0.001 μs suggesting that it has the highest

non-radiative energy loss. This is an interesting result as the data from both the PL and PLE studies suggest that Er(**3**)$_3$ has the most efficient energy transfer from the ligand into the Er^{3+} ion of all the complexes. The remaining complexes have longer radiative lifetimes ranging from approximately 1 μs to 1.7 μs and are presented in supplementary information Table S29.

After presenting the least efficient ligand sensitization (Figure 14(a)) it is found that Er(**4**)$_3$ has the longest radiative lifetime. This is evidence that the bromination is successful in reducing intra-atomic non-radiative relaxation but also reduces sensitization efficiency. The radiative lifetimes of the Er^{3+} complexes studied here are found to reduce upon the ligand substitution in the order 3,5-Br > dpa > chel > 4-Cl.

The PLQE of the Er(**1**-**4**)$_3$ were not calculated as the radiative emissions were found to be too weak to measure using the integrating sphere method. This places an upper limit on the PLQE of ~0.174 x 10^{-6} for all the Er^{3+} complexes, based on the lowest PLQE recorded during this work (from Nd(**2**)$_3$). As the PLQE complexes studied in this paper have followed a similar order to the PL lifetime we therefore predict the order of the PLQE for the Er^{3+} complexes to be 3,5-Br > dpa > chel > 4-Cl, with Er(**3**)$_3$ being the least efficient complex.

Judd-Ofelt theory was again used to analyze the absorption of the complexes, their oscillator strengths, emission probabilities and branching ratios were determined. Supplementary information Figure S12 shows the absorption spectrum for Er(**1**)$_3$ following correction for ligand absorption providing nine intra-atomic transitions for use in the modeling. The same procedure was used for Er(**2**-**4**)$_x$ again providing nine Er^{3+} transitions with the exception of Er(**4**)$_3$ where only seven were fully resolvable due to intense ligand absorption (Figure 14 (b)). Supplementary information Table S30 presents the integrated absorption cross-sections as well as measured and calculated oscillator strengths for each intra-atomic transition for Er(**1**)$_3$ complex. As with the previous complexes the Judd-Ofelt parameters were obtained and are presented in supplementary information Table S31. The values of ΔS_{rms} obtained for each complex suggests that the least squares fit is good for all cases with the highest deviation occurring for Er(**3**)$_3$ at a value of 0.31 x 10^{-20} cm^2. Further analysis including calculation of the fluorescence line strengths,

radiative decay rates, branching ratios and radiative lifetimes of several possible decay routes in the Er^{3+} ion are provided in supplementary information Table S32 info for completeness.

4. Discussion

The results presented above enable us to provide a clearer picture as to the potential of pyridine 2,6-dicarboxylate and its 4-substituted and 3,4,5-tri-substituted analogues for sensitization of Ln^{3+} PL. Key to this is the ability to build a picture of the ligand energy levels based on the variation of ligand emission as the various Ln^{3+} are complexed. Analysis of the results leads to the conclusion that the singlet level of Ln(**1**)$_3$ lies at ca. 3.1 eV (400 nm) resonant with the ($^4F_{7/2}$, $^4I_{13/2}$) level of Dy^{3+} and the $^2H_{9/2}$ level of Er^{3+} and placing it ca. 200 meV above the singlet level of Ln(**4**)$_3$. Similarly the triplet state of Ln(**1**)$_3$ must lie at ca. 2.6 eV (ca. 477 nm) resonant with the $^3P_0$ level of Pr^{3+}, the $^4G_{9/2}$ level of Nd^{3+}, the $^4F_{9/2}$ level of Dy^{3+} and the $^4F_{7/2}$ level of Er^{3+}. This places it ca. 250 meV above the triplet state of Ln(**4**)$_3$. Such a placement correlates well with previously reported work on Tb(**1**-**4**)$_3$ which indicated energy transfer to the Tb^{3+} state occurs via the singlet state.[20] The only Tb^{3+} energy level within the vicinity of the ligand states is the $^5D_4$ corresponding to an excitation energy of 2.57 eV (483 nm). This would only allow triplet sensitization from Tb(**1**)$_3$ as the remaining complexes have their triplet level below this and are therefore sensitized via their singlet state. Likewise by comparison with previous work on Eu(**1**-**4**)$_x$ we can see that the singlet state of Eu(**1**)$_3$ is resonant to the $^5D_3$ level whilst the triplet state is unable to sensitize the Eu^{3+} (Figure 3).[21] The absence of any ligand emission from this complex indicates therefore that efficient energy transfer occurs from the singlet state as previously predicted. Substitution to form Eu(**2**)$_3$ was found to reduce the sensitization although still no ligand emission was observed, which is attributed to quenching of the excited Eu^{3+} by the presence of the OH group. Based on the energy level alignment proposed sensitization may occur via the triplet state rather than the singlet however quenching is still likely to take place.

We have assumed that the metal plays only a very minor role in determining the ligand state energies in line with other studies.[28] In these studies a small variation in the ligand emission was observed (ca. 75

meV) when complexed to Eu^{3+} and Lu^{3+} neither of which could be sensitized. This was attributed to the smaller ionic radius of Lu^{3+} due to the well-known lanthanide contraction effect. A similar comparison of the ligand emission from the various Ln^{3+} complexes of **1** and **4** was carried out but energy transfer to the Ln^{3+} affects many of the spectra preventing any detailed analysis of this effect. However, comparison of the absorption spectra does not indicate any systematic shift due to variation of the Ln^{3+} ionic radius (supplementary information Figure S13).

The data presented above suggests that hypersensitivity of the Er^{3+} $^4I_{15/2} \rightarrow {}^2H_{11/2}$ (ca. 522 nm) and $^4I_{15/2} \rightarrow {}^4G_{11/2}$ (ca. 381 nm) was observed in the case of Er(**3**)$_3$. Though less clear, the reduction in the high energy side of the Dy^{3+} $^6H_{15/2} \rightarrow {}^6F_{11/2}$ (ca. 1087 nm) absorption in Dy(**3**)$_3$ also indicated that hypersensitivity may be occurring. Inspection of the Nd^{3+} $^4I_{9/2} \rightarrow {}^4G_{5/2}$ absorption (at ca. 580 nm) did not reveal any differences however. Those hypersensitive transitions of Gd^{3+} lie within the ligand absorption edge whilst those of Pr^{3+} lie at ca. 1920 nm and could not be observed.[50]

Finally, we present in Table 1 the relative Ln^{3+} emission intensity of each complex relative to that of Ln(**1**)$_3$. As would be expected the specifics vary for each Ln^{3+} and excitation energy chosen. For Pr^{3+} and Dy^{3+}, ligand substitution does not seem to provide any benefit in terms of sensitization efficiency of the Ln^{3+} emission. Inspection of the intra-atomic 4*f* energy levels for Dy^{3+} (Figure 3) illustrates that once an excited electron reaches the $^6F_{1/2}$ energy level it would be able to rapidly relax via non-radiative relaxation. We note that the use of ligands in which halogenation at the 4 or 3,5-position has been undertaken has a dramatic effect in reducing the relative strength of emission (Table 1). This is in agreement with the increase in phonon energy such halogenation provides facilitating non-radiative relation from the $^4F_{9/2}$ level to the $^6F_{1/2}$. In the case of Pr^{3+} the picture is more nuanced with the Pr(**3**)$_3$ complex yielding a lower relative emission from the Pr^{3+} ion (despite the increased sensitization implied by the PLE spectra in Figure 6a) than obtained from Pr(**4**)$_3$ where partial bromination has been performed. For Nd^{3+} and Er^{3+} significant improvement in the sensitization efficiency can be achieved via ligand substitution, aided by the reduction in non-radiative relaxation of the excited ions due to the partial chlorination or bromination

undetaken. In the case of Nd^{3+} a 4 to 5-fold increase in NIR emission is achieved with substitution using (**3**) or (**4**) even though in the case of (**4**) the Nd^{3+} is not fully coordinated by the ligand. For Er^{3+} characteristic emission is only obtained for $Er(\mathbf{2})_3$ when exciting at 351 nm. However, upon 458 nm excitation, similar to that of Nd^{3+}, an increase in NIR emission is achieved in the case of $Er(\mathbf{3})_3$ and $Er(\mathbf{4})_3$. To obtain quantitative details on the sensitization efficiency for each complex further work is required. However, the above reported results provide significant guidance to aid such work and to also guide the development of further modified ligand systems for improved Ln^{3+} sensitization and NIR emission.

Table 1. Relative strength of Ln^{3+} PL obtained under 351 nm and 458 nm excitation.

	Pr^{3+}		Nd^{3+}		Dy^{3+}		Er^{3+} [a]
λ_{ex}	351 nm	458 nm	351 nm	458 nm	351 nm	458 nm	458 nm
$(dpa)_x$	1.00	1.00	1.00	1.00	1.00	1.00	1.00
$(chel)_x$	0.11	0.40	0.84	1.03	1.04	0.11	0.35
$(4\text{-}Cl)_x$	0.16	0.08	4.72	0.96	0.04	0.03	1.10
$(3,5\text{-}Br)_x$	0.99	0.14	3.81	1.00	0.01	<0.01	2.39

[a]Excitation at 351 nm only yielded 1530 nm emission for $Er(\mathbf{2})_3$.

5. Conclusions

In this article we report the preparation and characterization of a series of Ln^{3+} complexes with pyridine 2,6-dicarboxylic acid (**1**) and its 4-substituted and 3,4,5-tri-substituted derivatives. Detailed spectroscopic analysis is provided and through rigorous examination of the observed behavior we are able to obtain a detailed understanding of ligand sensitization mechanisms that lead to excitation of a variety of coordinated Ln^{3+} ions including Pr^{3+}, Nd^{3+}, Dy^{3+} and Er^{3+}. Based on the ligand-based photoluminescence obtained from Gd^{3+}-complexes and the relative ligand and Ln^{3+} emission obtained from the other

complexes, the singlet and triplet state energies of complexes of (**1**) are estimated to be at 3.1 eV and 2.6 eV respectively whilst for the 3,5-dibromo-substituted complexes (**4**) they are at 2.9 eV and 2.3 eV. We additionally report the hypersensitivity of the Er^{3+} $^4I_{15/2} \rightarrow {}^2H_{11/2}$ and $^4I_{15/2} \rightarrow {}^4G_{11/2}$ intra-atomic transitions in the 4-chloro substituted (**3**) complex.

In carrying out this study we also demonstrate the ability to obtain sensitized emission throughout the majority of the NIR spectral range with continuous coverage across the 700 – 1100 nm and 1300 – 1650 nm region from a single family of complexes. This emission also includes the longest reported NIR emission from an organolanthanide complex to date at ca. 1855 nm from Dy(**1**)$_3$. Furthermore, complexes of (**1**) and the majority of the substituted ligands are found to fully satisfy the 8-9 coordination requirement of the Ln^{3+} ions. This is especially attractive for their utilization in aqueous systems including bio-sensing and low-cost sensing applications. In relation to identifying improved ligands for NIR emission we demonstrate a 5-fold increase in the emission of Nd^{3+} and 2-fold increase in the emission of Er^{3+} via substitution of (**1**) with (**3**) and (**4**) respectively.

Acknowledgements We thank the EPSRC for studentships to AJB, MRG and PEC.

Supporting information available. Synthesis and chemical characterization of Ln(**1-4**)$_x$. Additional absorption and PL spectra of various Ln(**1-4**)$_x$ complexes. Judd-Ofelt model validation and calculated parameters for each complex. Tabulated relative emission strengths, radiative lifetimes and PLQE values obtained for various Ln^{3+}. Full crystallographic details for all crystal structures are included in Table S1 and S2. CCDC 1916056-1916068 contain the supplementary crystallographic data for this paper. These data can be obtained free of charge from The Cambridge Crystallographic Data Centre via www.ccdc.cam.ac.uk/data_request/cif.

References

[1] S.I. Weissman, Intramolecular Energy Transfer the Fluorescence of Complexes of Europium. J. Chem. Phys. 10 (1942) 214-217.

[2] J. Kido, Y. Okamoto, Organo Lanthanide Metal Complexes for Electroluminescent Materials. Chem. Rev. 102 (2002) 2357-2368.

[3] E. Soini, T. Lovgren, T. Time-Resolved Fluorescence of Lanthanide Probes and Applications in Biotechnology. Crit. Rev. Anal. Chem. 18 (1987) 105-154.

[4] J.C.G. Bunzli, L.J. Charbonniere, R.F. Ziessel, Structural and Photophysical Properties of Ln(III) Complexes with 2,2'-bipyridine-6,6'-dicarboxylic Acid: Surprising Formation of a H-Bonded Network of Bimetallic Entities. J. Chem. Soc. Dalton Trans. 12 (2000) 1917-1923.

[5] R.J. Curry, W.P. Gillin, Electroluminescence of Organolanthanide Based Organic Light Emitting Diodes. Curr. Opin. Solid State Mater. Sci. 5 (2001) 481-486.

[6] G.A. Hebbink, L. Grave, L.A. Woldering, D.N. Reinhoudt, F.C.J.M. van Veggel, Unexpected Sensitization Efficiency of the Near-Infrared Nd^{3+}, Er^{3+}, and Yb^{3+} Emission by Fluorescein Compared to Eosin and Erythrosin. J. Phys. Chem. A 107 (2003) 2483-2491

[7] S. Quici, M. Cavazzini, G. Marzanni, G. Accorsi, N. Armaroli, B. Ventura, F. Barigelletti, Visible and Near-Infrared Intense Luminescence from Water-Soluble Lanthanide [Tb(III), Eu(III), Sm(III), Dy(III), Pr(III), Ho(III), Yb(III), Nd(III),, Er(III)] Complexes. Inorg. Chem. 44 (2005) 529-537

[8] L. Sun. H. Zhang, Q. Meng, F. Liu, L. Fu, C. Peng, J. Yu, G. Zheng, S. Wang, Near-Infrared Luminescence Hybrid Materials Doped with Lanthanide (Ln) Complexes (Ln = Nd, Yb) and Their Possible Laser Application. J. Phys. Chem. B 109 (2005) 6174-6182.

[9] W.P. Gillin, R.J. Curry, Erbium (III) tris(8-hydroxyquinoline) (ErQ):A Potential Material for Silicon Compatible 1.5 μm Emitters. Appl. Phys. Lett. 74 (1999) 798-799.

[10] R.J. Curry, W.P. Gillin, A.P. Knights, R. Gwilliam, 1.5 μm Electroluminescence From Organic Light Emitting Diodes Integrated on Silicon Substrates. Opt. Mater. 17 (2001) 161-163.

[11] L.H. Sloof, A.V. Blaaderen, A. Polman, G.A. Hebbink, S.I. Klink, F.C.J.M. van Veggel, D.N. Reinhoudt, J.W. Hofstraat, Rare-Earth Doped Polymers for Planar Optical Amplifiers. J. Appl. Phys. 91 (2002) 3955-3980.

[12] G.M. Davies, R.J. Aarons, G.R. Motson, J.C. Jeffery, H. Adams, S. Faulkner, M.D. Ward, Structural and Near-IR Photophysical Studies on Ternary Lanthanide Complexes Containing Poly(pyrazolyl)borate and 1,3-diketonate Ligands. J. Chem. Soc. Dalton Trans. (2004), 1136-1144.

[13] H. He, Near-Infrared Emitting Lanthanide Complexes of Porphyrin and BODIPY Dyes. Coord. Chem. Rev. 273-274 (2014) 87-99.

[14] J.C.G. Bunzli, S. Comby, A.S. Chauvin, C.D.B. Vandevyver, New Opportunities for Lanthanide Luminescence. J. Rare Earths 25 (2007) 257-274.

[15] S.V. Eliseeva, J.C.G. Bunzli, Lanthanide Luminescence for Functional Materials and Bio-Sciences. Chem. Soc. Rev. 39 (2010) 189-227.

[16] S. Lis, M. Elbanowski, B. Makowska, Z. Hnatejko, Energy Transfer in Solution of Lanthanide Complexes. J. Photochem. Photobio. A: Chem. 150 (2002) 233-247.

[17] J.C.G. Bunzli, On the Design of Highly Luminescent Lanthanide Complexes. Coord. Chem. Rev. 293 (2015) 19-47.

[18] G.A. Hebbink, S.I. Klink, L. Grave, P.G.B. Oude Alink, F.C.J.M. van Veggel, Singlet Energy Transfer as the Main Pathway in the Sensitization of Near-Infrared Nd^{3+} Luminescence by Dansyl and Lissamine Dyes. Chemphyschem 3 (2002) 1014-1018.

[19] A.P. de Silva, H.Q.N. Gunaratne, C.P. McCoy, Molecular Photoionic AND Logic Gates with Bright Fluorescence and “Off-On” Digital Action. J. Am. Chem. Soc. 119 (1997) 7891-7892.

[20] J.B. Lamture, Z.H. Zhou, A.S. Kumar, T.G. Wensel, Luminescence Properties of Terbium(III) Complexes with 4-Substitued Dipicolinic Acid Analoges. Inorg, Chem. 34 (1995) 864-869.

[21] M.R. George, C.A. Golden, M.C. Grossel, R.J. Curry, Modified Dipicolinic Acid Ligands for Sensitization of Europium(III) Luminescence. Inorg. Chem. 45 (2006) 1739-1744.

[22] A. Rodriguez-Rodriguez, D. Esteban-Gomez, A. de Blas, T. Rodriguez-Blas, M. Fekete, M. Botta, R. Tripier, C. Platas-Iglesias, Lanthanide(III) Complexes with Ligands Derived from a Cyclen Framework Containing Pyridinecarboxylate Pendants. The Effect of Steric Hindrance on the Hydration Number. Inorg. Chem. 51 (2012) 2509-2521.

[23] F. Mian, G. Bottaro, R. Seraglia, M. Cavazzini, S. Quici, L. Armelao, The Role of Ligand Topology in the Decomplexation of Luminescent Lanthanide Complexes by Dipicolinic Acid. ChemPhysChem 17 (2016) 3229-3236.

[24] M.L. Cable, J.P. Kirkby, D.J. Levine, M.J. Manary, H.B. Gray, A. Ponce, A. Detection of Bacterial Spores with Lanthanide-Macrocycle Binary Complexes. J. Am. Chem. Soc. 131 (2009) 9562-9570.

[25] Y. Zhang, B. Li, H. Ma, L. Zhang, H. Jiang, H. Song, L. Zhang, Y. Luo, A Nanoscaled Lanthanide Metal-Organic Framework as a Colorimetric Fluorescence Sensor for Dipicolinic Acid Based on Modulating Energy Transfer. J. Mater. Chem. C 4 (2016) 7294-7301.

[26] M. Wu, Y. Zhuang, J. Liu, W. Chen, X. Li, R.J. Xie, Radiometric Fluorescence Detection of 2,6-pyridine Dicarboxylic Acid with a Dual-Emitting Lanthanide Metal-Organic Framework (MOF). Opt. Mater. 106 (2020) 110006.

[27] X. Liu, D. Chen, C.C. Wang, N.J. Tian, Z.Q. Li, Y. Zhang, Z.J. Ding, A Turn-On Luminescence Probe for Highly Slective Detection of an Anthrax Biomarker. Lumin. 35 (2020) 601-607.

[28] A. D'Aleo, A. Picot, A. Beeby, J.A.G. Williams, B.L. Guennic, C. Andraud, O. Maury, Efficient Sensitiztion of Europium, Ytterbium, and Neodymium Functionalized Tris-Dipicolinic Lanthanide Complexes Through Tunable Charge-Transfer Excited States. Inorg. Chem. 47 (2008) 10258-10268.

[29] S.V. Eliseeva, G Aubock, F. van Mourik, A. Cannizzo, B. Song, E. Deiters, A. Chauvin, M. Chergui, J.C.G. Bunzli, Multiphoton-Excited Luminescent Lanthanide Bioprobes: Two- and Three-Photon Cross Sections of Dipicolinic Derivatives and Binuclear Helicates. Phys. Chem. B 114 (2010) 2932-2937.

[30] Z.E.A. Chama, X. Guo, J.L. Canet, A. Gautier, D. Boyer, R. Mahiou, Clicked Dipicolinic Antennae for Lanthanide Luminescent Probes. Dalton Trans. 39 (2010) 7091-7097.

[31] J. Andres, A.S. Chauvin, Energy Transfer in Coumarin-Sensitised Lanthanide Luminescence: Investigation of the Nature of the Sensitiser and its Distance to the Lanthanide Ion. Phys. Chem. Chem. Phys. 15 (2013) 15981-15994.

[32] H.J. Park, S.B. Ko, I.W. Wyman, S. Wang, Selective Sensitization of Eu(III) and Tb(III) Emission with Triarylboron-Functionalized Dipicolinic Aids. Inorg. Chem. 53 (2014) 9751-9760.

[33] M. Rasanen, J. Rosenberg, J. Lukkari, K. Haapakka, J. Kankare, H. Takalo, Study on Luminescent Ternary EuEDTA Complexes With a Set of Substituted 4-Phenylethynyl and 4-aryl Pyridine-2,6,dicarboxylic Acids. J Lumin. 187 (2017) 471-478.

[34] H. Chen, R. Shi, H. Ow, Predicting Stability Constants for Terbium(III) Complexes with Dipicolinic Acid and Substituted Dipicolinic Acid Analogues Using Density Functional Theory. ACS Omega 4 (2019) 20665-20671.

[35] M. Rasanen, H. Takalo, J. Rosenberg, K. Haapakka, J. Lukkari, J. Kankare, Energy Transfer in Ternary TbEDTA Chelates with a Series of Dipicolinic Acid Derivatives. J. Lumin. 222 (2020) 116967.

[36] B.R. Judd, Optical Absorption Intensities of Rare-Earth Ions. Phys. Rev. 127 (1962) 750-761.

[37] G.S. Ofelt, Intensities of Crystal Spectra of are-Earth Ions. J. Chem. Phys. 37 (1962) 511.

[38] B.M. Walsh, Advances in Spectroscopy for Lasers and Sensing, Springer Netherlands, 2006.

[39] J.C. de Mello, H.F. Wittmann, R.H. Friend, An Improved Experimental Determination of External Photoluminescence Quantum Efficiency. Adv. Matter. 9 (1997) 230-232.

[40] W.T. Carnall, P.R. Fields, K. Rajnak, Spectral Intensities of the Trivalent Lanthanides and Actinides in Solution. II. Pm^{3+}, Sm^{3+}, Eu^{3+}, Gd^{3+}, Tb^{3+}, Dy^{3+}, and Ho^{3+}. J. Chem Phys. 49 (1968) 4412-4423.

[41] W.T. Carnall, P.R. Fields, K. Rajnak, Electronic Energy Levels of the Trivlent Lanthanide Aquo Ions. I. Pr^{3+}, Nd^{3+}, Pm^{3+}, Sm^{3+}, Dy^{3+}, Ho^{3+}, Er^{3+}, and Tm^{3+}. J. Chem Phys. 49 (1968) 4424-4442.

[42] W.T. Carnall, P.R. Fields, K. Rajnak, Electronic Energy Levels of the Trivlent Lanthanide Aquo Ions. II. Gd^{3+}. J. Chem Phys. 49 (1968) 4443-4446.

[43] W.T. Carnall, P.R. Fields, K. Rajnak, Electronic Energy Levels of the Trivlent Lanthanide Aquo Ions. IV. Eu^{3+}. J. Chem Phys. 49 (1968) 4450-44455.

[44] J.R. Xie, V.H. Smith, R.E. Allen, Spectroscopic Properties of Dipicolinic Acid and its Dianion. Chem. Phys. 322 (2006) 254-268.

[45] A. Alimova, A. Katz, H.E. Savage, M. Shah, G. Minko, D.V. Will, R.B. Rosen, S.A. McCormick, R.R. Alfano, Native Fluorescence and Excitation Spectroscopic Changes in Bacillus Subtilis and Staphylococcus Aureus Bacteria Subjected to Conditions of Starvation. Appl. Opt. 42 (2003) 4080-4087.

[46] R. Nudelman, B.V. Bronk, S. Efrima, Fluorescence Emission Derived from Dipicolinic Acid, its Sodium, and its Calcium Salts. Appl. Spectrosc. 54 (2000) 445-449.

[47] A. Babai, A. Mudring, Anhydrous Praseodymium Salts in the Ionic Liquid [bmpyr][Tf_2N]: Structural and Optical Properties of [bmpyr]$_4$[PrI_6][Tf_2N] and [bmyr]$_2$[$Pr(Tf_2N)_5$]. Chem. Mater. 17 (2005) 6230-6238.

[48] A.M. Srivastava, Identification of the I^- to Pr^{3+} Charge Transfer Transition in the Excitation Spectrum of $LuI_3:Pr^{3+}$. Opt. Mater. 30 (2008) 1567-1570.

[49] B. Yan, W. Wang, Y. Song, Photophysical Properties of Praseodymium Complexes with Aromatic Carboxylic Acids: Double Light Conversion Both in Ultraviolet and Visible Region. Spectrocim. Acta A 66 (2007) 1115-1121.

[50] R.D. Peacock, The Intensities of Lanthanide f→f Transitions, in: E. Nieboer, C.K. Jørgensen, R.D. Peacock, R. Reisfeld, Rare Earths (Structure and Bonding 22), Springer-Verlag, Berlin, 1975, pp. 83-122.

[51] E.O. Serqueira, N.O. Dantas, A.F.G. Monte, M.J.V. Bell, Judd Ofelt Calculation of Quantum Efficiencies and Branching Ratios of Nd^{3+} Doped Glasses. J. Non-Cryst. Solids 352 (2006) 3628-3632.

[52] G. Wang, Optical-Transition Probability of the Nd^{3+} Ion in GdAl3(BO3)4 Crystal. J. Opt. Soc. Am. B 18 (2001) 173-175.

[53] J. Hölsä, R. Lamminmäki, P. Porcher, Simulation of the Energy Levels of Dy^{3+} in DyOCl. J. Alloys Compd. 275-277 (1998) 398-401.

[54] V.V. Apollonov, A.A. Pushkar', T.V. Uvarova, S.P. Chernov, Absorption of Dy^{3+} and Nd^{3+} Ions in BaR_2F_8 Single Crystals. Phys. Solid State. 50 (2008) 1660-1663.

[55] G. Lakshminarayana, J. Qiu, M.G. Brik, I.V. Kityk, Photoluminescence of Eu^{3+}-, Tb^{3+}-, Dy^{3+}- and Tm^{3+}-Doped Transparent GeO_2-TiO_2-K_2O Glass Ceramics. J. Phys. Condens. Matter. 20 (2008) 335106.

[56] R. Faoro, M. Tonelli, N. Magnani, E. Cavalli, Energy Levels and Emission Parameters of the Dy^{3+} Ion Doped into the YPO_4 Host Lattice. J. Phys. Condens. Matter. 21 (2009) 275501.

[57] W.T. Carnall, The Near Infrared Transitions of the Trivalent Lanthanides in Solution. II. Tb^{3+}, Dy^{3+}, Ho^{3+}, Er^{3+}, Tm^{3+}, and Yb^{3+}. J. Phys. Chem. 67 (1963) 1206-1211.

[58] M.B. Saisudha, J. Ramakrishna, Effect of Host Glass on the Optical Absorption Properties of Nd^{3+}, Sm^{3+}, and Dy^{3+} in Lead Borate Glasses. Phys. Rev. B 53 (1996) 6186-6196.

[59] Y.G. Choi, R.J. Curry, B.J. Park, K. Kim, J. Heo, D.W. Hewak, Extreme Hypersensitivity Observed from $^6H_{15/2}$ to $^6F_{11/2}$ Transition of Dy^{3+} in Inorganic Noncrystalline Solids. Chem. Phys. Let. 403 (2005) 29-34.

[60] Y.G. Choi, R.J. Curry, B.J. Park, K.H. Kim, J. Heo, D.W. Hewak, D. W. Controlling Fluorescence Lifetime of Rare-Earth Element in Amorphous Inorganic Solids Via Very Small Compositional Adjustments. J. Appl. Phys. 98 (2005) 023523.

[61] D.K. Sardar, W.M. Bradley, R.M. Yow, J.B. Gruber, B. Zandi, Optical Transitions and Absorption Intensities of Dy^{3+} ($4f^9$) in YSGG Laser Host. J. Lumin. 106 (2004) 195–203.

[62] D.G. Karraker, Hypersensitive Transitions of Hydrated Nd^{3+}, Ho^{3+}, and Er^{3+} Ions. Inorg. Chem. 1968, 7, 473-479; Isobe, T.; Misumi, S. Spectral Intensities of Some Er^{3+} β-Diketonate Complexes. Bull. Chem. Soc. Jpn. 47 (1974) 281-284.